NTNU

Norwegian University of
Science and Technology

Control of VSC-HVDC for wind power

Chandra Bajracharya

Master of Science in Energy and Environment
Submission date: June 2008
Supervisor: Marta Molinas, ELKRAFT

Norwegian University of Science and Technology
Department of Electrical Power Engineering

Problem Description

North of Norway has extremely good conditions for wind power generation. As the existing main grid will not be able to integrate all the wind parks, the alternative to build a new corridor with multi-terminal HVDC Light from North of Norway to Middle of Norway, is under study.

HVDC Light is more and more concerned recently to improve power system stability due to its supreme controllability. The thesis will be directed towards investigating the possible problems to be encountered in an HVDC Light installation. A platform for the control of HVDC Light based on the vector control principle will be first established. With a good understanding of this control platform, the model will then be tested under several circuit conditions, to test the capability and robustness of the controller to handle these situations.

Assignment given: 21. January 2008
Supervisor: Marta Molinas, ELKRAFT

Abstract

With the recent developments in semiconductors and control equipment, Voltage Source Converter based High Voltage Direct Current (VSC-HVDC) has attracted the growing interest of researchers. The use of VSC technology and Pulse Width Modulation (PWM) has a number of potential advantages: short circuit current reduction; rapid and independent control of the active and reactive power, etc. With such highly favourable advantages, VSC-HVDC is definitely going to be a large part of future transmission and distribution systems. HVDC technology based on VSC technology has been an area of growing interest recently because of its suitability in forming a transmission link for transmitting bulk amount of wind power.

This thesis deals with the control of VSC-HVDC. The objective of the work is to understand the control structure of the VSC-HVDC system, and establish the tuning criteria for the PI controllers of the converter controllers.

A model of a VSC based dc link using PWM Technology is developed. A mathematical model of the control system based on the relationships between voltage and current is described for the VSC. A control system is developed combining an inner current loop controller and outer dc voltage controller. The vector control strategy is studied and corresponding dynamic performance under step changes and system fault is investigated in PSCAD/EMTDC simulation package. The simulation results verify that the model can fulfill bi-directional power transfers, fast response control and that the system has good steady state performance. The controller parameters tuned according to the developed tuning criteria is found to provide acceptable system performances.

Abbreviations

HVAC	:	High Voltage Alternating Current
HVDC	:	High Voltage Direct Current
VSC	:	Voltage Source Converter
CSC	:	Current Source Converter
IGBT	:	Insulated Gate Bipolar Transistor
PWM	:	Pulse Width Modulation
PI control	:	Proportional plus Integral control
ac/AC	:	Alternating current
dc/DC	:	Direct Current
PLL	:	Phase Lock Loop

Contents

Abstract

Abbreviations

Chapter 1 Introduction

1.1 Background 1

1.2 Problem Definition 2

1.3 Objectives of the Study 3

1.4 Contribution of Thesis Work 3

Chapter 2 High Voltage DC Transmission

2.1 Introduction 4

2.2 Classical HVDC System 4

2.2.1 Configuration of classic HVDC 4

2.2.2 Advantages of classic HVDC 6

2.3 VSC-HVDC System 6

2.3.1 Configuration 6

2.3.2 Control and Operating Principle 7

2.3.3 Difference from classic HVDC and Advantages 9

Chapter 3 Control System

3.1 Introduction 12

3.2 Vector Control Principle 13

3.2.1 DQ Transformation 13

3.2.2 Vector Control 14

3.3 Inner Current Controller 17

3.3.1 System Description and Transfer Function 17

3.3.1.1 PI Regulator 18

3.3.1.2 PWM Converter 18

3.3.1.3 The System 18
3.3.1.3 Control Block Diagram 20
3.3.2 Per Unit Representation of transfer function 21
3.3.3 Tuning of Controller 21
3.3.3.1 Modulus Optimum Tuning Criteria 22
3.3.3.2 Tuning of Current Controller using Modulus Optimum 22
3.4 The Outer Controller 23
3.4.1 System Description and Transfer Function 23
3.4.1.1 PI Regulator 24
3.4.1.2 The current Controller 24
3.4.1.3 The System 24
3.4.1.4 The Feedforward 25
3.4.1.5 Control Block Diagram 26
3.4.2 Per Unit Representation of transfer function 26
3.4.3 Tuning of Controller 27
3.4.3.1 Symmetrical Optimum Tuning Criteria 28
3.4.3.2 Tuning of dc-voltage controller using Symmetric Optimum 28
3.4.3.3 Pole placement interpretation of Symmetrical Optimum 29
3.4.3.4 Tuning of dc-voltage controller using Pole placement 31
3.4.4 Active and Reactive power controller 31

Chapter 4 Simulation and Results

4.1 Test System 33
4.2 Transfer function analysis 34
4.2.1 Current controller tuning by modulus optimum 34
4.2.1.1 Frequency domain analysis 34
4.2.1.2 Time domain analysis 35
4.2.2 DC voltage controller tuning by symmetric optimum 36
4.2.2.1 Frequency domain analysis 37
4.2.2.2 Time domain analysis 38
4.2.3 DC voltage controller tuning by pole placement 38

4.2.3.1 Frequency domain analysis 39
4.2.3.2 Time domain analysis 39
4.3 Simulation Results 40
4.3.1 Case 1: Transients in dc Voltage 41
4.3.2 Case 2 : Change in reactive power 43
4.3.3 Case 3: Change in active power load 45
4.3.4 Case 4: Unbalance fault conditions 47

Conclusion 49
Further Work 50
References 51
Appendix

Chapter 1

Introduction

1.1 Background

North of Norway has extremely good conditions for establishment of wind power generation farms. It has been seen that there is a possibility of about 4000MW of wind power generation in this area. Integration of massive amounts of wind power, as high as 4000MW is a major challenge to the power industry, one of the big issues being how to collect the wind power and feed it into the ac grid.

The main grid in Northern Norway consists of a weak 132 kV network, and the transmission lines, will not be able to handle and export the surplus energy from these areas to the consumption areas in the middle of Norway. As the existing main grid will not be able to integrate all the generated wind power, alternative methods are being to be considered for the integration of this new energy into the existing system.

Two alternative methods are available for the connection of wind farms to the grid, high voltage ac (HVAC) and high voltage dc (HVDC). For an optimum result, all possible alternatives need to be analysed keeping in view, the system requirement and the future expansion of the system. Although HVAC provides simplest and most economic connection method for short distances, HVDC transmission becomes the only feasible option for connection of a wind farm when the distance exceeds 100-150km [1]. HVDC traditionally has been used to transfer large amounts of power over long distances. But for traditional HVDC the reactive power cannot be controlled independently of the active power.

The HVDC technology based on voltage source converters (VSC), has recently been an area of growing interest due to a number of factors, like its modularity, independence of ac network, independent control of active and reactive power, low power operation and power reversal etc. The voltage source technologies also facilitate the connection of several converters to a common dc-bus, forming an HVDC grid [2].

VSC based HVDC systems incorporate the control strategy based on vector control, which is most widely used in the control of three phase pulse width modulated (PWM) converters. In PWM converters for ac applications, vector control systems can be utilized to obtain independent control of the active and reactive powers.

1.2 Problem Definition

In PWM converters for ac applications, vector control systems can be utilized to obtain independent control of the active and reactive powers. The characteristics of vector control, as will be described in Chapter 3, is that vectors of ac currents and voltages occur as constant vectors in steady state, and hence static errors in the control system can be avoided by using PI controllers.

The design of controllers is based on two tasks; determining the structure of the controller and adjusting the controller's parameters to give an optimal system performance. The design is normally done with complete knowledge of the system, which is normally described by a linear, time invarient, continuous or discrete time model. The structure and parameters of the controller are chosen such that the system's response can meet certain qualitative criteria; stable response, appropriate disturbance handling capabilites, robustness and speed etc.

The PI controller is the most commonly used control algorithm. PI controllers have traditionally been tuned empirically. There also exist some tuning rules developed to be used for the design of these controllers for industrial applications, electric drives. Design of PI controllers is important because of the significant impact it may give to system response. An efficient design method should be able to provide robust controller parameters. Adequate performance of VSC-HVDC

system under diverse operating conditions depends on the selection of robust parameters for the control system.

1.3 Objectives

The thesis is basically focused on the analysis of the control structure. The objectives of the study are mentioned below:

- Develop an understanding of the control strategy for VSC based HVDC (Vector control)
- Establish the transfer function for the controllers
- Establish the tuning rules for the controllers based on the transfer function structure
- Verify the stability/robustness of controllers through simulation
- Understand the effect of choice of controller parameters on its performance

1.4 Contribution of Thesis Work

Following the objectives mentioned, this thesis studies the control scheme for a VSC-HVDC link connecting two grids.

A mathematical model of a voltage source converter is presented in synchronous rotating frame. The method presented assumes a linear process whose dynamics is characterized in terms of a transfer function. The model is used to analyze voltage and current control loops for the VSC. Vector control principle is used for decoupled control of active and reactive power, and transfer functions in per unit are derived for the control loops.

In investigating the operating conditions for HVDC systems, the tuning of controllers is one of the critical stages of the design of control loops. Three tuning techniques are discussed in this thesis and analytical expressions are derived for calculating the parameters of the current and voltage controllers. The “modulus” and “symmetric” optimization techniques are two methods for designing “optimal” linear control systems in the frequency domain, which are considered in this thesis. The tuning criteria are discussed and simulations are used to test the performance of such tuning techniques.

Chapter 2

High Voltage DC Transmission

2.1 Introduction

High voltage DC transmission is a high power electronics technology used in electric power systems. It is an efficient, economic and flexible method to transmit large amounts of electrical power over long distances by overhead transmission lines or underground/submarine cables. Factors such as improved transient stability, dynamic damping of electrical system oscillations and possibility to interconnect two systems at different frequencies influence the selection of dc transmission over ac transmission.

Until recently HVDC transmission based on thyristors, which is called traditional HVDC or classic HVDC, was used for conversion from ac to dc and vice versa. The HVDC transmission based on voltage source converters (VSC) is a comparatively new technology, where the valves are built by IGBTs (Insulated Gate Bipolar Transistors) and PWM (Pulse Width Modulation) is used to create the desired voltage waveform. The technology is commercially available as HVDC light [2] and HVDC plus [3].

2.2 Classic HVDC Systems

2.2.1 Configuration of classic HVDC systems

A classic HVDC system operating in bipolar mode is shown in Fig. 2.1, which consists of ac filters, shunt capacitor banks or other reactive-compensation equipment, converter transformers, converters, dc reactors, dc filters, and dc lines or cables. Classic HVDC converters are current source converters (CSC). The CSCs perform the conversion from ac to dc (rectifer) at the sending end and from dc to ac (inverter) at the receiving end. The dc current is kept constant and

magnitude and direction of power flow are controlled by changing magnitude and direction of dc voltage.

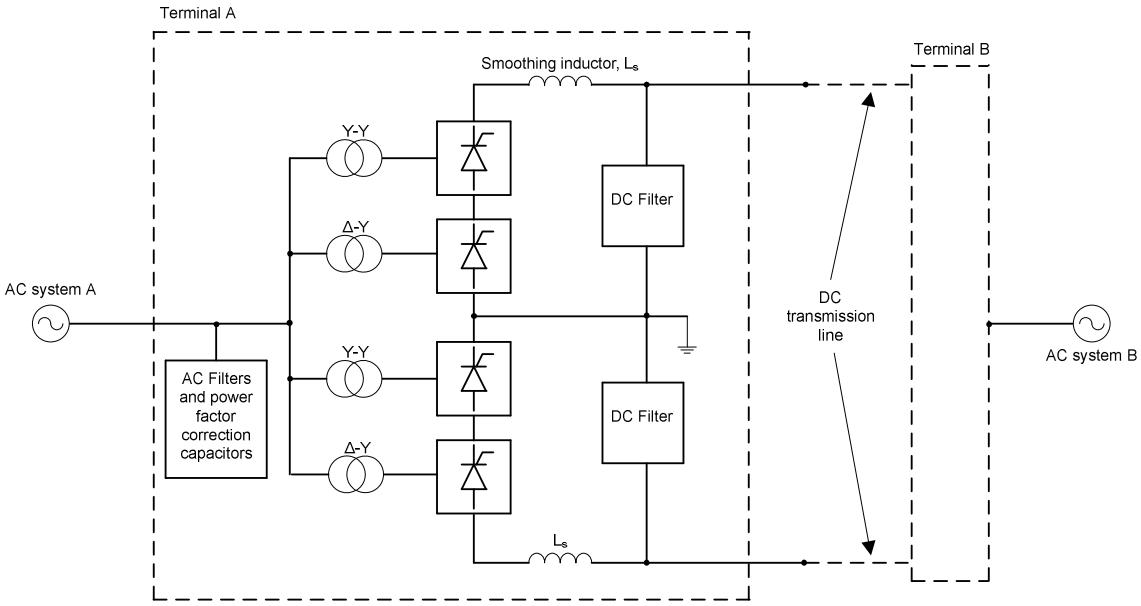

Figure 2.1 – Basic configuration for a classic HVDC transmission system

Each converter terminal in Fig. 2.1 consists of a positive and a negative pole. Each pole consists of two six pulse bridges connected through converter transformers with winding structures Y-Y and Δ-Y, forming a 12-pulse converter bridge. Such arrangement results in the 5^{th} and 7^{th} harmonic currents to be in opposite phases, thus reducing the distortion in ac system [4]. The current harmonics generated by the converters are prevented from entering into the connected ac network by ac filters. In the conversion process the converter consumes reactive power which is compensated in part by the filter banks and the rest by capacitor banks. Dc filters and smoothing inductors reduce the ripple produced in dc transmission line current.

The power transmitted over the HVDC link is controlled through the control system where one of the converters controls the dc voltage and the other converter controls the current through the dc circuit. The control system acts through firing angle adjustments of the valves and through tap changer adjustments on the converter transformers to obtain the desired combination of voltage and current. Power reversal is obtained by reversing polarity of direct voltages at both ends. The

control systems of the two stations of a bipolar HVDC system usually communicate with each other through a telecommunication link.

2.3.2 Advantages of Classic HVDC Systems

An HVDC system has a lot of value added to transmission of electrical power than in the case of using conventional ac transmission. Some of these aspects are:

- No limits in transmission distance.
- Very fast and accurate control of power flow, implying stability improvements, for the HVDC link as well as the ac system.
- Bi-directional power flow
- An HVDC link does not increase the short-circuit power in the connecting point.
- The need for right-of-way is much smaller for HVDC than for an ac connection, for the same transmitted power. The environmental impact is therefore smaller with HVDC, and it is easier to obtain permission to build.
- Power can be transmitted between two ac-systems operating at different nominal frequencies or at the same frequency but without being synchronized.

2.3 VSC-HVDC system

2.3.1 Configuration

Fig. 2.2 shows the basic structure of the VSC based HVDC link, consisting of two converters, dc-link capacitors, passive high-pass filters, phase reactors and dc cable. The VSCs as shown in Fig. 2.2 are composed of six-pulse bridge equipped with self commutating switches (IGBTS) and diodes connected in anti parallel. The dc voltage is maintained constant and the complexity of control is increased compared to classical HVDC system.

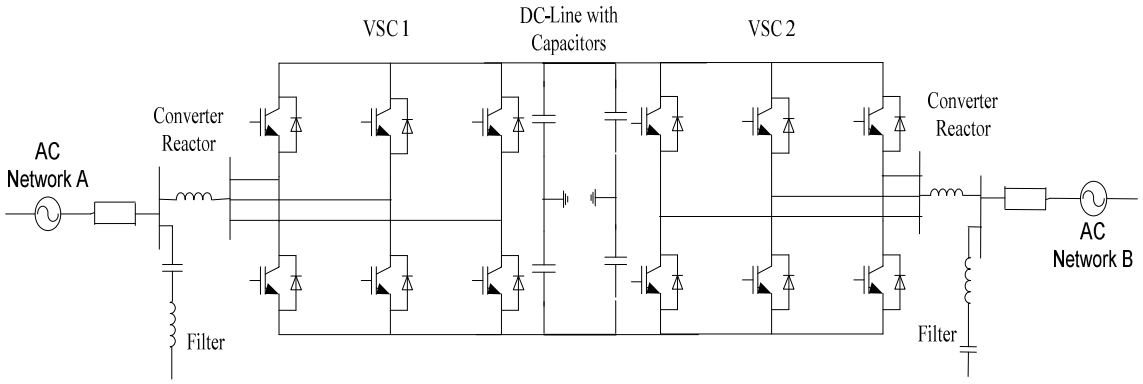

Figure 2.2 – Basic configuration of VSC based HVDC transmission system

The phase reactors as shown in Fig. 2.2 are used for controlling both the active and the reactive power flow by regulating currents through them. High pass filter branches prevent the harmonics due to switching of the IGBT's from being emitted into the ac system. The dc capacitors provide a low inductive path for the turn-off current and acts as energy storage. The capacitor reduces the voltage ripple on the dc side, and the size of these capacitors depends on the required dc voltage. By using Pulse Width Modulation techniques with high switching frequency in the range of 1-2 kHz, the wave shape of the converter ac voltage output can be controlled to be almost sinusoidal with the aid of high frequency filter. Changes in waveform, phase angle and magnitude can be made by changing the PWM pattern, which can be done almost instantaneously [5]. Thus, the voltage source converter can be considered as a controllable voltage source. This high controllability allows for a wide range of applications. From a system point of view VSC-HVDC acts as a synchronous machine without mass that can control active and reactive power almost instantaneously. And as the generated output voltage can be virtually at any angle and amplitude with respect to the bus voltage, it is possible to control the active and reactive power flow independently.

2.3.2 Control and Operating Principle of VSC-HVDC

The fundamental operation of VSC-HVDC may be explained by considering the terminal of voltage source connected to the ac transmission network via filters as shown in Fig. 2.3.

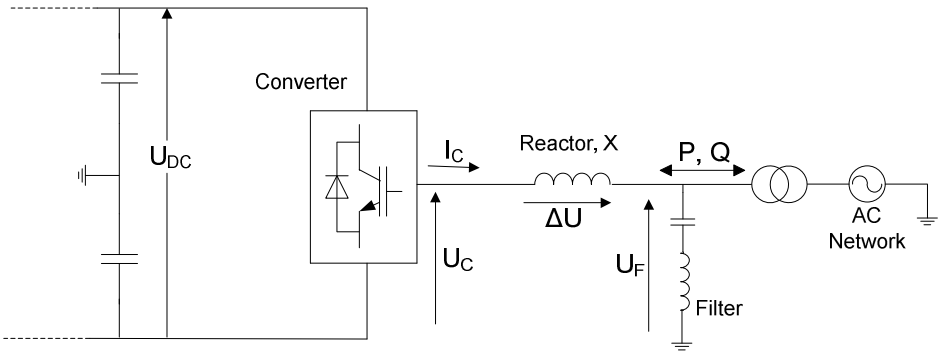

Figure 2.3 – Simplified circuit diagram

The voltage source converter can be considered as a fast controllable synchronous machine whose fundamental frequency output voltage is given by,

$$(U_C)_1 = \frac{1}{2} m_a . U_{dc} . Sin(\omega t + \phi) \tag{2.1}$$

Where m_a is modulation index, ω is the fundamental frequency and φ is the phase shift of the output voltage, U_C.

Taking the voltage at the filter bus U_F as reference, the power transfer from the converter to the ac system can be written as,

$$P = \frac{U_F . U_C . Sin\phi}{X} \tag{2.2}$$

$$Q = \frac{U_F . (U_F - U_C . Cos\phi)}{X} \tag{2.3}$$

With the pulse width modulation, the variables m_a and φ can be adjusted independently by the VSC controller to give any combination of voltage magnitude and phase shift. It is therefore possible to control the voltage drop across the reactor and hence the active and reactive power flows. Power can be controlled by changing the phase angle of the converter ac voltage with respect to the filter bus voltage whereas the reactive power can be controlled by changing the magnitude of fundamental component of converter ac voltage with respect to filter bus voltage. By controlling these two aspects, the converter can be operated in all the four quadrants of P-Q characteristics [6,7]. The limitations to the capability arise only because of the maximum current

through IGBT switches, maximum dc voltage level and the maximum dc current through dc cable.

Being able to independently control ac voltage magnitude and phase relative to the system voltage allows the use of separate active and reactive power control loops for HVDC system regulation. The active power control loop can be set to control either the active power or the dc side voltage. In VSC-HVDC connections, the active power flow on the ac side is equal to the active power transmitted from dc side in steady state, disregarding the losses. This can be fulfilled if one of the two converters controls the active power transmitted and the other controls dc voltage. The reactive power control loop can be set to control either the reactive power or the ac side voltage. Either of the two modes can be selected independently at either end of the dc link. Fig. 2.4 shows the principle control of HVDC transmission for one terminal.

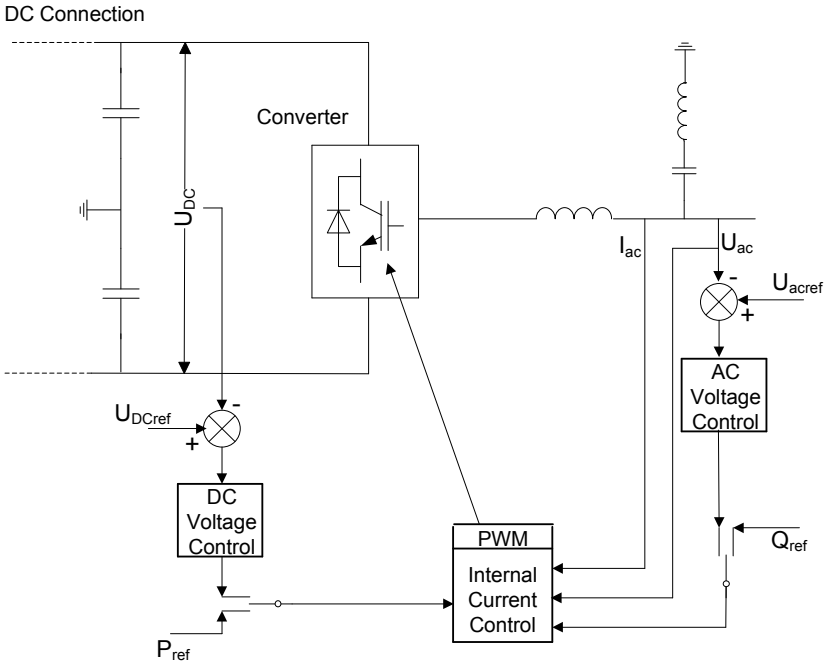

Figure 2.4 – Principle Control of VSC-HVDC

2.3.3 Difference from classical HVDC and Advantages

The main difference in operation between classic HVDC and VSC-HVDC is the higher controllability of the latter. This leads to a number of new advantages and applications, some of which are given below [5,6].

- Classic HVDC terminals can provide limited control of reactive power by means of switching of filters and shunt banks and to some level by firing angle control. But this control requires additional equipment and therefore extra cost. With PWM, VSC-HVDC offers the possibility to control both active and reactive power independently. Hence independent control of active and reactive power is possible without any needs for extra compensating equipment.
- The reactive power capabilities of VSC-HVDC can be used to control the ac network voltages, and thereby contribute to an enhanced power quality. Furthermore, the faster response due to increased switching frequency(PWM) offers new levels of performance regarding power quality control such as flicker and mitigation of voltage dips, harmonics etc.
- HVDC Light does not rely on the AC network's ability to keep the voltage and frequency stable. Independence of ac network makes it less sensitive for disturbances in the ac network and ac faults do not drastically affect the dc side. If ac systems have ground faults or short circuits, whereupon the ac voltage drops, the dc power transmitted is automatically reduced to a predetermined value. Hence there is no contribution to the short circuit currents.
- By controlling grid voltage level, VSC can reduce losses in the connected grid.
- Disturbances in the ac system may lead to commutation failures in classic HVDC system. As VSC-HVDC uses self-commutating semiconductor devices, the risk of commutation failures is significantly reduced.
- The control systems on rectifier and inverter side operate independently of each other. They do not depend on a telecommunication connection. This improves the speed and the reliability of the controller.
- The VSC converter is able to create its own ac voltage at any predetermined frequency, without the need for rotating machines. HVDC Light can feed load into a passive network.
- VSC converters are very suitable for creating a dc grid with a large number of converters, since very little coordination is needed between the interconnected VSCs.

- Transient overvoltages can be counteracted by fast reactive power response. Thus stability margins are enhanced because of reactive power support. Moreover, the grid can be operated closer to upper limit, and higher voltage level allows more power transfer.
- Unlike conventional HVDC converters, VSC can operate at very low power. As the active and reactive power are controlled independently, even at zero active power, the full range of reactive power can be utilized. Active power transfer can be quickly reversed without any change of control mode, and without any filter switching or converter blocking. The power reversal is obtained by changing the direction of the DC current and not by changing the DC voltage as for conventional HVDC.

Chapter 3

Control System

3.1 Introduction

The control of a VSC-HVDC system is basically the control of the transfer of energy. The aim of the control in VSC based HVDC transmission is thus, the accurate control of transmitted power and independent control of active and reactive power.

Different control strategies are found in literature for the control of VSC-HVDC. One of the methods for control of VSC-HVDC is known as Direct Power Control (DPC) method. DPC is based on the instantaneous active and reactive power control loops [8]. In DPC there are no internal current control loops and no PWM modulator block, because the converter switching states are selected by a switching table based on the instantaneous errors between the commanded and estimated values of active and reactive power. This method uses estimated virtual flux vector in its control loop. Due to disadvantages like variable switching frequency and necessity of fast conversion and computation, the use of this type of control is not very common.

Another widely used method for control of VSC-HVDC is the vector control method. Vector control method uses modelling of three phase systems by using axis transformations. Vector theory is most widely used in the control of three phase PWM converters these days. In PWM converters for ac applications, vector control systems can be utilized to obtain independent control of the active and reactive powers. One of the most advantageous characteristics of vector control is that vectors of ac currents and voltages occur as constant vectors in steady state, and hence static errors in the control system can be avoided by using PI controllers.

3.2 Vector Control Principle

Vector control system involves simplified representation of three phase systems known as DQ transformations.

3.2.1 DQ Transformation

DQ transformation is the transformation of coordinates from the three-phase stationary coordinate system to the d-q rotating coordinate system. This transformation is made in two steps:

- a transformation from the three-phase stationary coordinate system to the two-phase, α-β stationary coordinate system and
- a transformation from the α-β stationary coordinate system to the d-q rotating coordinate system.

Clark and Inverse-Clark transformations are used to convert the variables (e.g. phase values of voltages and currents) into stationary α-β reference frame and vice-versa. Similarly, Park and Inverse-Park transformations convert the values from stationary α-β reference frame to synchronously rotating d-q reference frame, and vice versa.. The reference frames and transformations are shown in Fig.3.1.

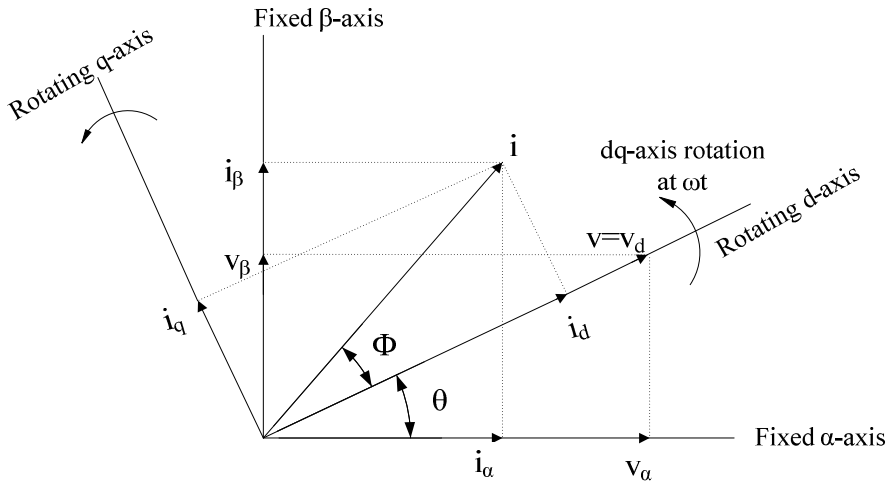

Figure 3.1 – Transformation of axes for vector control

The stationary α-axis is chosen to be aligned with stationary three phase a-axis for simplified analysis. The d-q reference frame is rotating at synchronous speed ω with respect to the

stationary frame α-β, and at any instant, the position of d-axis with respect to α-axis is given by θ=ωt. The summary of the transformation is presented in tabular form in Appendix-A. The transformation of axes in different control stages is shown in Fig.3.2.

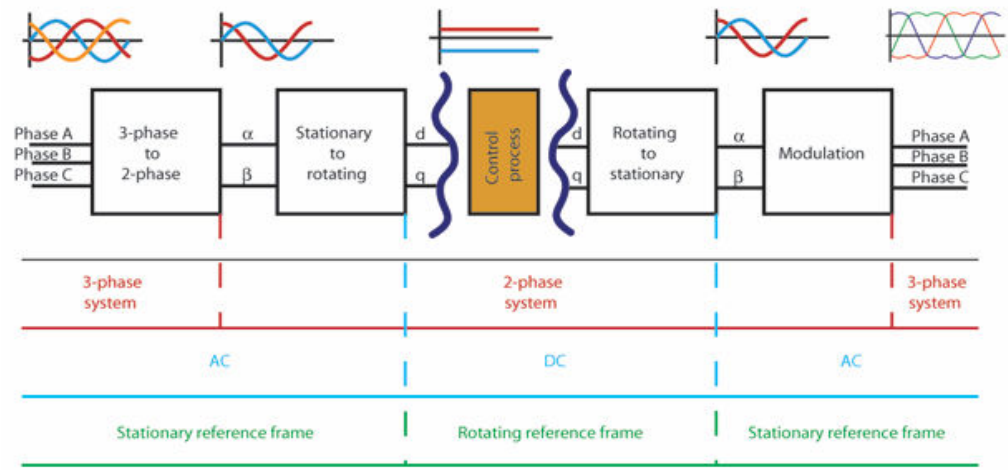

Figure 3.2 - Control Stages and respective reference frames

3.2.2 Vector Control

For analysis of the voltage source converter using vector control, three phase currents and voltages are described as vectors in a complex reference frame, called α-β frame. A rotating reference frame synchronized with the ac-grid is also introduced, as in Fig.3.1. As the d-q frame, is synchronized to the grid, the voltages and currents occur as constant vectors in the d-q reference frame in steady state, as depicted in the example of DQ-transformation in Appendix-B.

For the analysis of the system, basic equations describing the system behavior are presented based on analysis done in [9]-[11]. Considering the converter system connected to grid, and defining grid voltages as v_{abc}, currents i_{abc}, and converter input voltages $v_{abc\ conv}$, and resistance (R) and inductance (L) between the converter and the grid, as shown in the system of Fig.3.3, the voltage at the grid side of the converter can be expressed as,

$$v_{abc} = R.i_{abc} + L\frac{d}{dt}i_{abc} + v_{abc,conv} \qquad (3.1)$$

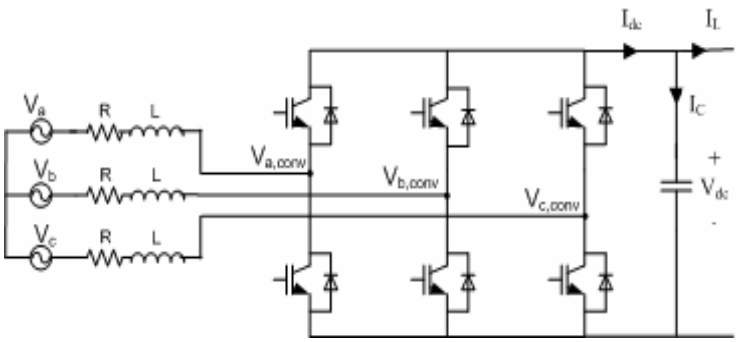

Figure 3.3 – Schematic of the System

Using the a-b-c to d-q transformations, the converter 3-phase currents and voltages are expressed in 2-axis d-q reference frame, synchronously rotating at given ac frequency, ω.

$$\begin{vmatrix} v_d \\ v_q \end{vmatrix} = R \begin{vmatrix} i_d \\ i_q \end{vmatrix} + L \frac{d}{dt} \begin{vmatrix} i_d \\ i_q \end{vmatrix} + L \begin{vmatrix} 0 & -\omega \\ \omega & 0 \end{vmatrix} \begin{vmatrix} i_d \\ i_q \end{vmatrix} + \begin{vmatrix} v_{dconv} \\ v_{qconv} \end{vmatrix} \tag{3.2}$$

The voltage equations in d-q synchronous reference frame are,

$$\begin{aligned} L \frac{di_d}{dt} &= -R i_d + \omega L i_q - v_{dconv} + v_d \\ L \frac{di_q}{dt} &= -R i_q - \omega L i_d - v_{qconv} + v_q \end{aligned} \tag{3.3}$$

Similarly on the output side,

$$I_{dc} = C . \frac{dV_{dc}}{dt} + I_L \tag{3.4}$$

The power balance relationship between the ac input and dc output is given as,

$$p = \frac{3}{2}(v_d . i_d + v_q . i_q) = V_{dc} . I_{dc} \tag{3.5}$$

where V_{dc} and I_{dc} are dc output voltage and current respectively.

The grid voltage vector is defined to be along the d-axis direction, and then a virtual grid flux vector can be assumed to be acting along the q-axis. With this alignment, $v_q = 0$ and the instantaneous real and reactive power injected into or absorbed from ac system is given by,

$$\begin{aligned} p &= \frac{3}{2} . v_d . i_d \\ q &= -\frac{3}{2} . v_d . i_q \end{aligned} \tag{3.6}$$

Hence, the transformation into rotating d-q coordinate system oriented with respect to the grid voltage vector, leads to a split of the mains current into two parts. One part determines the contribution which gives required power flow into the dc bus while the other part defines the reactive power condition. The system equation Eqn.(3.6) show directly the possibility to control two current components independently.

The angle between the α-axis of α-β frame and d-axis of the d-q frame is used for transformation between the α-β frame and d-q frame. The angular position of the voltage vector is given by,

$$\theta = \tan^{-1}\left(\frac{v_\beta}{v_\alpha}\right) \tag{3.7}$$

where v_α and v_β are components of voltage in stationary two axis reference frame, α-β. The information on this instantaneous phase angle of the grid voltage is very necessary for independent control of active and reactive power. The value of the angle θ is computed by using a synchronization technique, namely, phase lock loop (PLL) [12]-[13]. The information from phase lock loop is used to synchronize the turning on/off of the power devices, calculate and control the flow of active/reactive power by transforming the feedback variables to a reference frame suitable for control purposes.

The overall scheme of vector based control is as shown in Fig.3.4.

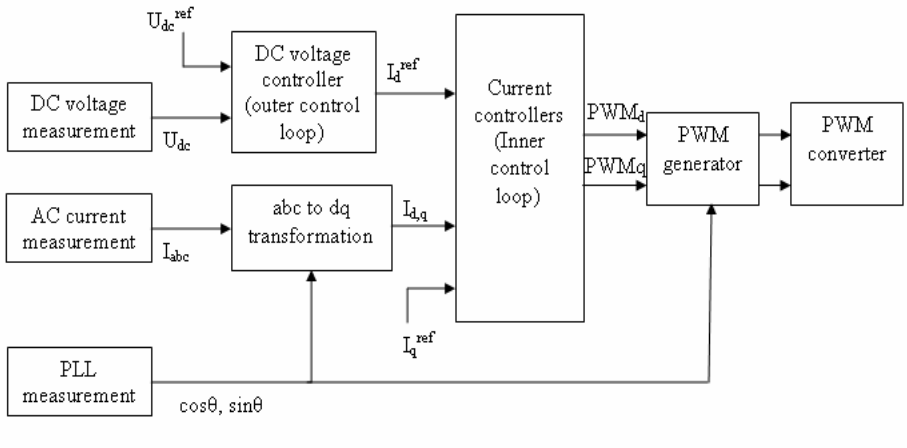

Figure 3.4 - Vector control principle

As the vector control technique offers decoupled control of active and reactive power and a fast dynamics, it makes the realization of system control in form of cascade structure possible, with two PI control loops in cascade, outer control loop and inner current control. The control system is based on a fast inner current control loop controlling the ac current. The ac current references are supplied by outer controllers. The outer controllers include the dc voltage controller, the active power controller, the reactive power controller and the ac voltage controller, depending upon the application. The reference value for active current can be provided by dc voltage controller or the active power controller, while the reference value for reactive current is provided by ac voltage controller or reactive power controller. In all the combinational cases of outer controllers, the dc voltage controller is necessary to achieve an active power balance in the system.

3.3 Inner Current Controller

3.3.1 System Description and Transfer Functions

The inner current control loop can be implemented in the dq-frame, based on the basic relationship of the system model. The control loop consists of PI controllers, decoupling factors and feed-forward terms as will be described further. The current control block is represented by the following general block diagram.

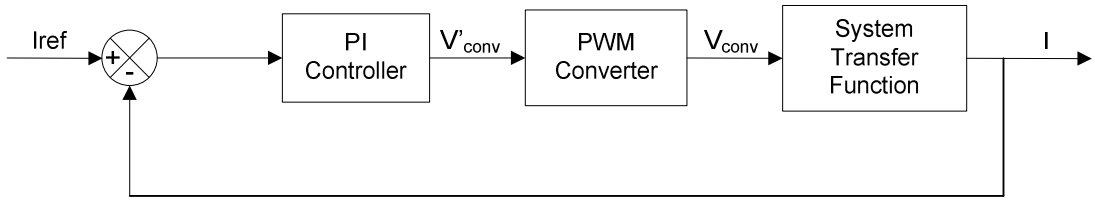

Figure 3.5 - General Block Diagram of Inner Current Control

Inside the current control block, there are two PI regulators, respectively for d and q axis current control. They transform the error between the comparison of d and q components of current into voltage value. In order to have a detail overview of the control system, each block of the control system is discussed as below.

3.3.1.1 PI Regulator

The representative equation of the PI regulator is:

$$R(s) = K_p + \frac{K_i}{s} = K_p \cdot \left(\frac{1 + T_i \cdot s}{T_i \cdot s} \right) \tag{3.8}$$

Where the proportional gain K_p and integral time constant $T_i = K_p / K_i$ are the design parameters to be specified. Thus for PI controller block,

$$\{I_{ref}(s) - I(s)\} \left(K_p + \frac{K_i}{s} \right) = V'_{conv}(s) \tag{3.9}$$

3.3.1.2 PWM Converter

From the control point of view, the converter is considered as an ideal power transformer with a time delay. The output voltage of the converter is assumed to follow a voltage reference signal with an average time delay equals half of a switching cycle, due to VSC switches. Hence the general expression is:

$$Y(s) = \frac{1}{1 + T_a \cdot s} \tag{3.10}$$

where $T_a = T_{switch} / 2$. Thus for converter block,

$$V'_{conv}(s) . \frac{1}{(1 + sT_a)} = V_{conv}(s) \tag{3.11}$$

3.3.1.3 The System

The system behaviour is governed by Eqn.(3.3) as described in Section 3.2.3. As seen from the equation, the model of the VSC in the synchronous reference frame is a multiple-input multiple-output, strongly coupled nonlinear system. And it is difficult to realize the exact decoupled control with general linear control strategies.

The transformed voltage equations of each axis have speed/frequency induced term (ωLi_d and ωLi_q) that gives cross-coupling between the two axes. For each axis, the cross-coupling term can be considered as disturbance from control point of view. Thus, a dual-close-loop direct current controller with decoupled current compensation and voltage feed-forward compensation is required to obtain a good control performance.

The system equations of Eqn.(3.3) are rewritten as follows,

$$\begin{aligned} v_d - v_{dconv} &= L\frac{di_d}{dt} + Ri_d - \omega L i_q \\ v_q - v_{qconv} &= L\frac{di_q}{dt} + Ri_q + \omega L i_d \end{aligned} \tag{3.12}$$

Using separate inner loop current controllers for i_d and i_q, give the output of voltage reference signals for two axes, which fed to the converter gives two references for the system, that are d-q components of $V_{conv}(s)$: V_{dconv} and $V_{qconv.}$. Using Eqn.(3.9) and Eqn.(3.11), these references are,

$$\begin{aligned} V_{dconv} &= \left(i_{dref} - i_d\right).\left(Kp + \frac{Ki}{s}\right).\frac{1}{(1+sT_a)} \\ V_{qconv} &= \left(i_{qref} - i_q\right).\left(Kp + \frac{Ki}{s}\right).\frac{1}{(1+sT_a)} \end{aligned} \tag{3.13}$$

As seen from Eqn.(3.12), the d and q components of the converter voltages are cross coupled. Hence, the reference used as input to system can be split in two components, one of which is obtained from converter whereas the other is a feed-forward term to eliminate the cross-coupling. With the compensation terms used for decoupling, the system input from converter is defined as

$$\begin{aligned} V'_{dconv} &= -\left(i_{dref} - i_d\right).\left(Kp + \frac{Ki}{s}\right) + \omega L i_q + v_d \\ V'_{qconv} &= -\left(i_{dref} - i_d\right).\left(Kp + \frac{Ki}{s}\right) - \omega L i_d + v_q \end{aligned} \tag{3.14}$$

Eqn.(3.14) when substituted in Eqn.(3.11) and equated to system equation Eqn.(3.12), it gives,

$$\begin{aligned} L\frac{di_d}{dt} + Ri_d &= V_{dconv} \\ L\frac{di_q}{dt} + Ri_q &= V_{qconv} \end{aligned} \tag{3.15}$$

The cross coupling terms are thus cancelled out and independent control in d and q axis is achieved, which is one of the important features of vector control. Thus current controllers of each axis operate independently.

As seen from Eqn. (3.15) the equations in d and q axis have a similar form. For this reason only the d-axis equations are used for further analysis. Consequently the other controller will also have the same parameters. By Laplace transformation the equation becomes:

$$s \cdot i_d(s) = -\frac{R}{L} \cdot i_d(s) + \frac{1}{L} \cdot V_{dconv}(s) \tag{3.16}$$

Thus, $$i_d(s) = \frac{1}{s \cdot L + R} \cdot V_{dconv}(s) \tag{3.17}$$

Hence the system transfer function is:

$$G(s) = \frac{1}{R} \cdot \frac{1}{1 + s \cdot \tau} \tag{3.18}$$

Where the time constant of the line is defined as $\tau = L/R$.

3.3.1.4 Control Block Diagram

The detailed block diagram of the complete system can be developed based on Eqn.(3.9), (3.11), (3.12), and (3.13) as shown in Fig.3.6.

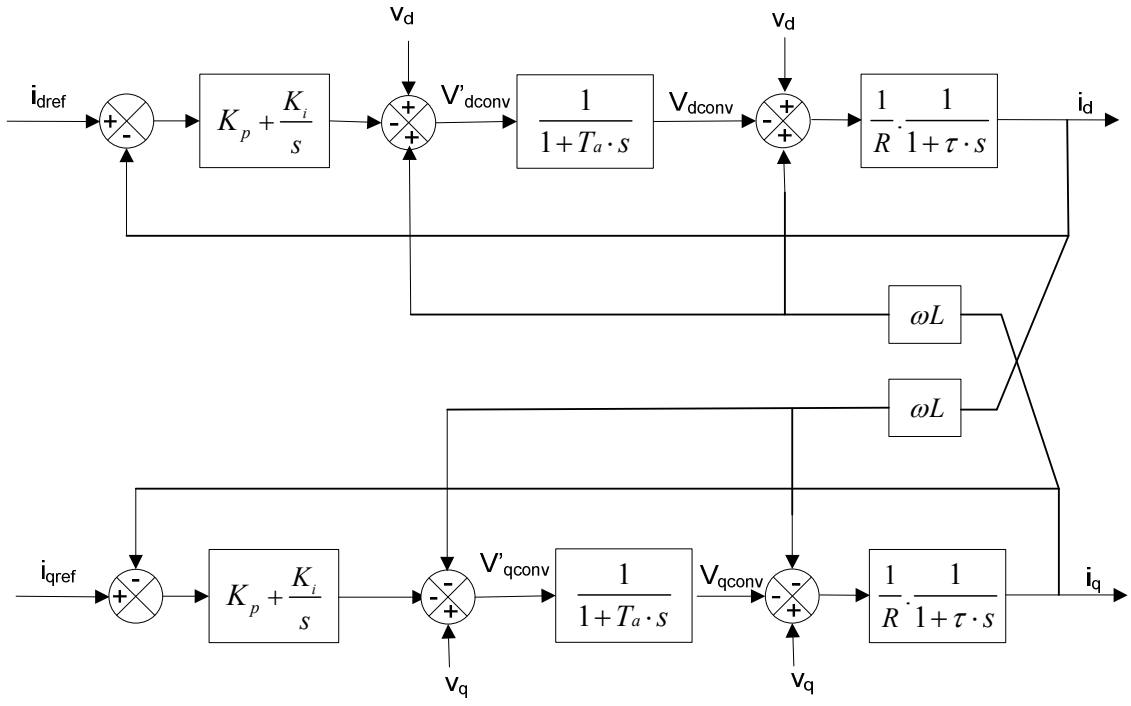

Figure 3.6 - Detail Block diagram of the complete system

But as shown in Eqn.(3.15), the feed-forward compensation term cancels the cross-coupling and hence there are two independent loops in d and q axis as shown in Fig.3.7.

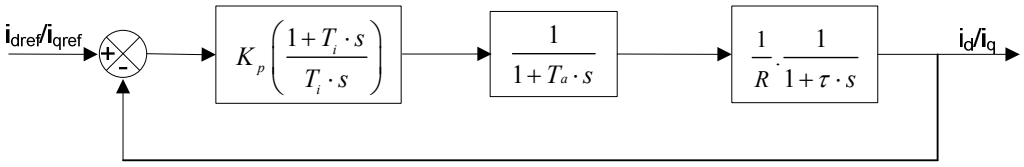

Figure 3.7 - Reduced block diagram in d and q axes

3.3.2 Per Unit Representation of Transfer Function

The base system for conversion of given system to per unit is given in the Appendix-C. Using the base system, the system equation Eqn.(3.15) is converted to per-unit as follows:

$$L.s\cdot i_{d,pu}(s).I_b + R\cdot i_{d,pu}(s).I_b = V_{dconv,\,pu}(s).V_b \tag{3.19}$$

$$L.s\cdot i_{d,pu}(s).\frac{I_b}{V_b} + R\cdot i_{d,pu}(s).\frac{I_b}{V_b} = V_{dconv,\,pu}(s) \tag{3.20}$$

$$\frac{L_{pu}}{\omega_b}.s\cdot i_{d,pu}(s) + R_{pu}\cdot i_{d,pu}(s) = V_{dconv,\,pu}(s) \tag{3.21}$$

The per unit inductance and resistance are defined as,

$$L_{pu} = \omega_b.L.\frac{I_b}{V_b} \quad \text{and} \quad R_{pu} = R.\frac{I_b}{V_b} \tag{3.22}$$

Hence, the per unit transfer function of the system becomes,

$$\frac{i_{d,pu}(s)}{V_{dconv,\,pu}(s)} = \frac{1}{R_{pu}}.\frac{1}{1+(L_{pu}/\omega_b.R_{pu}).s} = \frac{1}{R_{pu}}.\frac{1}{1+\tau_{pu}.s} \tag{3.23}$$

With the system transfer function expressed in per unit, the controller parameters will also be used in per unit ($K_{p,pu}$ and $T_{i,}$) in the controller transfer function.

3.3.3 Tuning of Controller

In the tuning process of PI controllers for VSC-HVDC, the tuning is done following the criteria adopted for electric drives [14]. Cascade control requires the speed of response to increase towards the inner loop. Hence, internal loop is designed to achieve fast response. The inner loop is tuned according to “modulus optimum” condition because of fast response and simplicity. This method provides a relatively fast and non-oscillatory closed-loop tracking response.

3.3.3.1 Modulus Optimum Tuning Criteria

For low order controlled plants without time delay the modulus optimum (absolute value optimum criterion) is often used in the conventional analog controller tuning. When the controlled system has one dominant time constant and other minor time constant, the standard form of the control system transfer function for the modulus optimum is achieved by cancelling the largest time constant, while the closed loop gain should be larger than unity for as high frequencies as possible [15]. This method is widely used because of its simplicity and fast response.

3.3.3.2 Tuning of Current Controller using Modulus Optimum

From the control block diagram of Fig.3.7 and the per unit representation formulated in Section 3.3.2, the open loop transfer function of the system can be written as,

$$G_{C,OL}(s) = K_{p,pu} \cdot \left(\frac{1 + T_i \cdot s}{T_i \cdot s} \right) \cdot \frac{1}{1 + T_a \cdot s} \cdot \frac{1}{R_{pu}} \cdot \frac{1}{1 + s \cdot \tau_{pu}} \tag{3.24}$$

As per modulus optimum tuning criteria, cancellation of slow process pole is done by the controller zero. Hence, simplifying the expression by defining $T_i = \tau_{pu}$, that is, eliminating the zero of the regulator, the open loop transfer function becomes,

$$G_{C,OL}(s) = \frac{K_{p,pu}}{\tau_{pu} \cdot R_{pu}} \cdot \frac{1}{s \cdot (1 + T_a \cdot s)} \tag{3.25}$$

Based on the open loop transfer function Eqn.(3.25), because of pole-zero cancellation, the closed lop transfer function becomes a second order transfer function given by Eqn.(3.26).

$$G_{C,CL}(s) = \frac{K_{p,pu} \Big/ \tau_{pu} \cdot R_{pu} \cdot T_a}{s^2 + 1 \Big/ T_a \cdot s + K_{p,pu} \Big/ \tau_{pu} \cdot R_{pu} \cdot T_a} \tag{3.26}$$

The system has undamped natural frequency $\omega_n = \sqrt{\frac{K_{p,pu}}{\tau_{pu} \cdot R_{pu} \cdot T_a}}$ and damping factor $\zeta = \frac{1}{2} \cdot \sqrt{\frac{\tau_{pu} \cdot R_{pu}}{K_{p,pu} \cdot T_a}}$.

The controller gain is calculated from the condition,

$$\left|\frac{G_{C,OL}(j\omega)}{1+G_{C,OL}(j\omega)}\right| = \left|\frac{K_{p,pu}}{\tau_{pu}\cdot R_{pu}.T_a.(j\omega)^2 + \tau_{pu}\cdot R_{pu}.(j\omega)+1}\right| = 1 \tag{3.27}$$

When the gain condition of Eqn.(3.27) is evaluated, the gain $K_{p,pu} = \frac{\tau_{pu}\cdot R_{pu}}{2\cdot T_a}$ .By using this value of gain, the closed loop transfer function is simplified as

$$G_{C,CL}(s) = \frac{1}{2T_a{}^2 s^2 + 2T_a\cdot s + 1} \tag{3.28}$$

where $\omega_n = \frac{1}{T_a\sqrt{2}}$ and $\zeta = \frac{1}{\sqrt{2}}$.

Hence the tuning of current controller by modulus optimum criteria can be summed up as,

$$K_{p,pu} = \frac{\tau_{pu}\cdot R_{pu}}{2\cdot T_a} \quad \text{and} \quad T_i = \tau_{pu} \tag{3.29}$$

3.4 The Outer Controller

3.4.1 System Description and Transfer Functions

In the thesis, the dc voltage controller is discussed as the outer controller. Dimensioning of the dc link voltage controller is determined by the transfer function between the current reference value to be given and the dc link voltage. The general block diagram of the external controller can thus be given as in Fig.3.8. The analysis of each component in block diagram follows in subsequent sections.

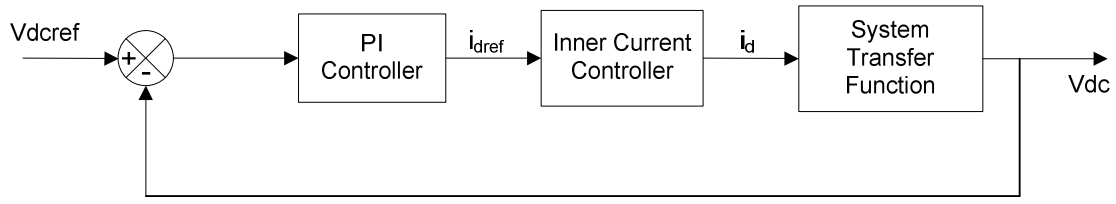

Figure 3.8 – General Block Diagram of Outer dc Voltage Control

3.4.1.1 PI Regulator

The representative equation of the PI regulator is:

$$R(s) = K_{pv} + \frac{K_{Iv}}{s} = K_{pv} \cdot \left(\frac{1 + T_{iv} \cdot s}{T_{iv} \cdot s} \right) \tag{3.30}$$

where the subscript "v" denotes the voltage regulator.

The controller parameters K_{pv} and $T_{iv} = K_{pv} / K_{iv}$ need to be designed for an optimum performance. For the PI controller block for outer voltage control,

$$\{V_{dcref}(s) - V_{dc}(s)\} \left(K_{pv} + \frac{K_{iv}}{s} \right) = i_{dref}(s) \tag{3.31}$$

3.4.1.2 The Current Controller

The closed current loop gives the relation between i_{dref} and i_d in the block diagram as in Fig.3.7. In many cases, the closed current loop is assumed to be ideal and represented by unity for design of outer loop. Instead of assuming the controller to be ideal, a simplified representation of the second order closed loop transfer function of the current controller by the equivalent first order approximation is considered here. The simplification is found by requiring the time integral of the difference between the reference and the output of the system after a reference step input to be equal for both the original second order model and the approximated one. The calculation behind the simplification is presented in Appendix-D. The simplification of the closed loop current controller transfer function as in Eqn.(3.28), by equivalent first order transfer function is,

$$\frac{1}{2T_a^2 s^2 + 2T_a \cdot s + 1} \cong \frac{1}{T_{eq} \cdot s + 1} \tag{3.32}$$

where $T_{eq} = 2T_a$.

3.4.1.3 The System

As discussed in Section 3.2.2, from the power balance equation, Eqn.(3.5) and using the condition $v_q = 0$, the relation between i_d and I_{dc} can be written as,

$$I_{dc} = \frac{3}{2} \cdot \frac{v_d}{V_{dc}} \cdot i_d \tag{3.33}$$

This defines the value of the current gain to be used from dc current to input current or vice versa. Substituting this value in Eqn.(3.4), we get,

$$C \cdot \frac{dV_{dc}}{dt} = \frac{3}{2} \cdot \frac{v_d}{V_{dc}} \cdot i_d - I_L \tag{3.34}$$

It is possible to observe that the DC-Link current equation is a non-linear equation. For analyzing the stability of a nonlinear system in the neighbourhood of a steady state operating point, it is necessary to linearize the system model around the operating point and perform linear stability analysis. The reference point for linearization is found by specifying reference input (V_{dcref}) for the nonlinear model.

The linearization is based on a Taylor series expansion of nonlinear function f around steady-state reference point (x_0, y_0 , z_0). The linear approximation is given by:

$$\frac{dx}{dt} = f(x,y,z) \Rightarrow \frac{d\Delta x}{dt} = \frac{\partial f}{\partial x}\Big|_{\substack{y=y_0 \\ z=z_0}} \cdot \Delta x + \frac{\partial f}{\partial y}\Big|_{\substack{x=x_0 \\ z=z_0}} \cdot \Delta y + \frac{\partial f}{\partial z}\Big|_{\substack{x=x_0 \\ y=y_0}} \cdot \Delta z \tag{3.35}$$

where x_0, y_0 and z_0 correspond to the initial condition.

The linearized form of the dc-link equation around the stationary system operating point is then:

$$C\frac{d\Delta V_{dc}}{dt} = \frac{3}{2} \cdot \frac{v_{d,0}}{V_{dc,ref}} \cdot \Delta i_d + \frac{3}{2} \cdot \frac{i_{d,0}}{V_{dc,ref}} \cdot \Delta v_d - \left(\frac{3}{2} \cdot \frac{v_{d,0} \cdot i_{d,0}}{V_{dc,ref}^2}\right) \cdot \Delta V_{dc} - \Delta I_L \tag{3.36}$$

To simplify this equation it needs to be observed that the only input of interest in the system equation is i_d, whereas, I_L acts as a disturbance. Consequently the linear expression becomes:

$$C\frac{d\Delta V_{dc}}{dt} = \frac{3}{2} \cdot \frac{v_{d,0}}{V_{dc,ref}} \cdot \Delta i_d \tag{3.37}$$

By Laplace transformation it is:

$$\frac{\Delta V_{dc}(s)}{\Delta i_d(s)} = \frac{3}{2} \cdot \frac{v_{d,0}}{V_{dc,ref}} \cdot \frac{1}{s \cdot C} \tag{3.38}$$

3.4.1.4 The Feed-forward

Although simple to design and implement, a cascade control system is likely to respond to changes more slowly than a control system where all the system variables are processed and acted upon simultaneously. The feed-forward is used to minimize disadvantage of slow dynamic response of cascade control. As the reference values of the inner loop variables are often available, these are fed forward for a faster and safe operation.

It has an advantage that the load variation can be greatly reduced and the large gain of voltage controller otherwise required to reduce this effect of large error is not necessary, which is important from stability viewpoint.

The dc link voltage controller controls the capacitor current so as to maintain the power balance. Hence under balanced conditions, I_c =0. That is, $I_{dc} = I_L$.

Thus, the reference value of i_d should be,

$$i_d = \frac{2}{3} \cdot \frac{V_{dc}}{v_d} \cdot I_L \tag{3.39}$$

which is the feed-forward term, ensuring exact compensation for load variation.

3.4.1.5 Control Block Diagram

The overall control block diagram of the dc voltage controller based on Eqn.(3.31)- (3.39) is as shown in Fig.3.9.

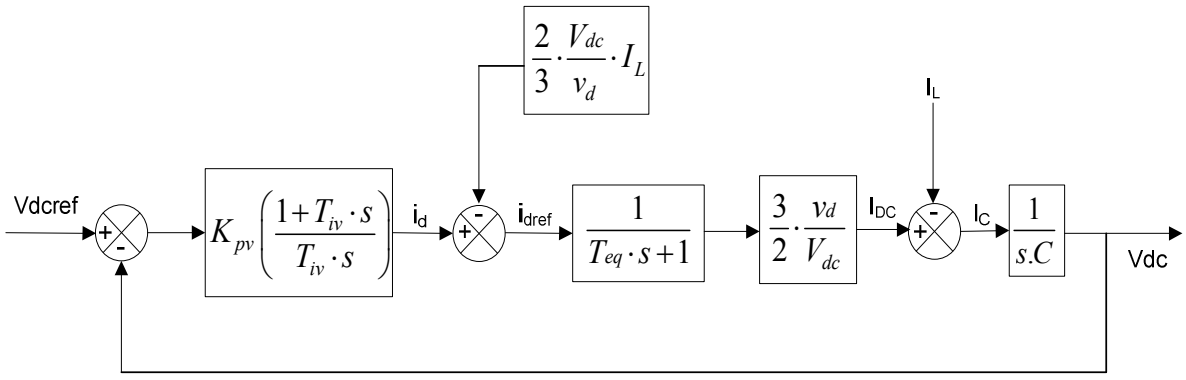

Figure 3.9 - Detail Block diagram of the complete system

3.4.2 Per Unit Representation of Transfer Function

Using the base system as given in Appendix-B, the power balance of Eqn.(3.32) can be converted to per unit as,

$$I_{dcpu}.I_{dcbase} = \frac{3}{2} \cdot \frac{v_{dpu}.V_b}{V_{dcpu}.V_{dcbase}} \cdot i_{dpu}.I_b \tag{3.40}$$

Because the base for per unit conversion is chosen to be power invariant (Base power at ac side = Base power at dc side), the current gain simplifies as,

$$I_{dcpu} = \frac{v_{dpu}}{V_{dcpu}} \cdot i_{dpu} \tag{3.41}$$

The dynamic equation of the dc-link in per unit is derived from Eqn.(3.4) as follows,

$$\frac{1}{\omega_b . C_{pu} . Z_{dcbase}} \cdot \frac{dV_{dcpu}}{dt} . V_{dcbase} = (I_{dcpu} - I_{Lpu}) . I_{dcbase} \tag{3.42}$$

The per unit capacitance is defined as, $C_{pu} = \frac{1}{\omega_b . C . Z_{dcbase}}$

Then Eqn.(3.42) simplifies as,

$$\frac{1}{\omega_b . C_{pu}} \cdot \frac{dV_{dcpu}}{dt} = (I_{dcpu} - I_{Lpu}) \tag{3.43}$$

By using Laplace transform, the equation takes the form,

$$V_{dcpu}(s) = \frac{\omega_b . C_{pu}}{s} (I_{dcpu}(s) - I_{Lpu}(s)) \tag{3.44}$$

Similarly the feed-forward function in per unit becomes,

$$i_{dpu} = \frac{V_{dcpu}}{v_{dpu}} \cdot I_{Lpu} \tag{3.45}$$

The control block diagram in per unit is shown in Fig.3.10.

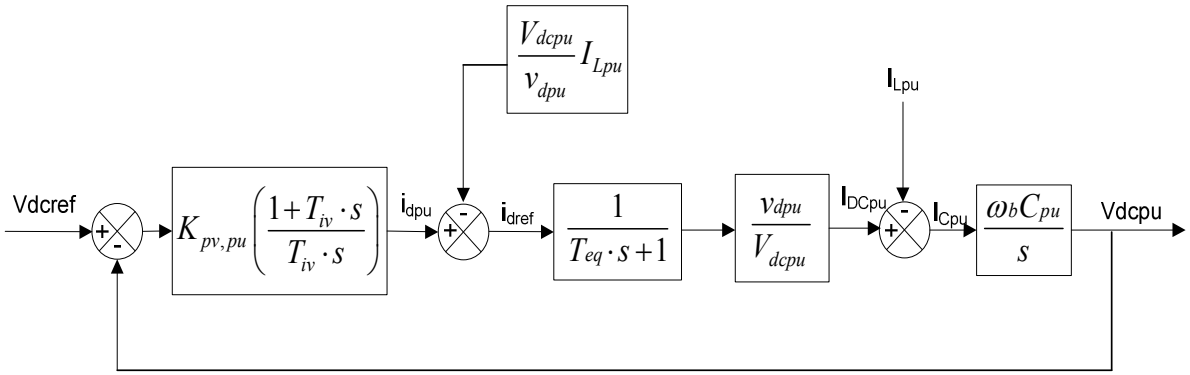

Figure 3.10 - Block diagram of the complete system in per unit

3.4.3 Tuning of Controller

As described in Section 3.3.3, the internal current control loop is designed to achieve fast response. On the other hand, main design goals of outer loop are optimum regulation and

stability. In cascade control, generally the inner loop is tuned according to "modulus optimum" condition because of fast response and simplicity whereas the outer loop according to "symmetrical optimum" condition for optimizing system behaviour with respect to disturbance signals [16].

3.4.3.1 Symmetrical Optimum Tuning Criteria

When the controlled has one dominant time constant and other minor time constant, the PI controller can be tuned using the modulus optimum criteria as described in Section 3.3.3. However, when one of the poles is already near to the origin or at the origin itself, the pole shift does not change the situation significantly. The open loop transfer function of the outer dc voltage controller already has two poles at the origin, as will be discussed in next section. Hence an alternative criterion to tune the controllers in this condition is given by the symmetrical optimum criteria.

A symmetrical optimum design criterion obtains a controller that forces the frequency response of the system as close as possible to that for low frequencies. The method has the advantage of maximizing the phase margin. As phase margin is maximized for given frequency, the system can tolerate more delays, which is important for systems having delays. This method optimizes the control system behaviour with respect to disturbance input. The method has well established tuning rules and has good disturbance rejection [17,18]. An extended approach of tuning by symmetric optimum [18] is presented here.

3.4.3.2 Tuning of dc-voltage controller using Symmetric Optimum

From the system block diagram as developed in Fig.3.10, the open loop transfer function of the system without considering the feed-forward and the disturbance input is given by,

$$G_{V,OL}(s) = K_{pv,pu} \cdot \left(\frac{1 + T_{iv} \cdot s}{T_{iv} \cdot s} \right) \cdot \frac{1}{1 + T_{eq} \cdot s} \cdot \left(\frac{v_{dpu}}{V_{dcpu}} \cdot \frac{\omega_b . C_{pu}}{s} \right) \tag{3.46}$$

The open loop transfer function consists of double pole at origin. The system cannot be designed by cancelling the pole and zero, because it will result in two poles at origin and the system becomes unstable. Hence the design is chosen by using symmetrical optimum design criteria. Symmetrical Optimum method obtains a controller that forces the frequency response from a reference point to output as close as possible to that for low frequencies. The method has the

advantage of maximizing the phase margin. As phase margin is maximized for given frequency, the system can withstand more delay, which is important for systems having delays. This method optimizes the control system behaviour with respect to disturbance input.

Eqn.(3.46) can be simplified by introducing $K = v_d / V_{dc}$, and $T_c = 1/\omega_b.C_{pu}$ as follows.

$$G_{V,OL}(s) = K_{pv,pu} \cdot \left(\frac{1 + T_{iv} \cdot s}{T_{iv} \cdot s} \right) \cdot \frac{K}{1 + T_{eq} \cdot s} \cdot \left(\frac{1}{s \cdot T_c} \right) \tag{3.47}$$

For a better understanding, derivation of the tuning criteria is presented in Appendix-E. According to the tuning criteria derived, the parameters for tuning the outer controller by symmetrical optimum are,

$$T_{iv} = a^2.T_{eq} \quad \text{and} \quad K_{pv,\,pu} = \frac{T_c}{K.\sqrt{T_{iv}.T_{eq}}} = \frac{T_c}{a.K.T_{eq}} \tag{3.48}$$

Using the parameters, the open loop transfer function becomes,

$$G_{V,OL}(s) = \frac{1}{a^3.T_{eq}{}^2.s^2} \cdot \left(\frac{1 + a^2.T_{eq}.s}{1 + T_{eq}.s} \right) \tag{3.49}$$

And the closed loop transfer function is then,

$$G_{v,CL}(s) = \frac{1 + a^2.T_{eq}.s}{1 + a^2.T_{eq}.s + a^3.T_{eq}{}^2.s^2 + a^3.T_{eq}{}^3.s^3} \tag{3.50}$$

3.4.3.3 Pole placement interpretation of Symmetrical Optimum

As seen from Eqn.(3.50), the denominator of the closed loop transfer function using symmetric optimum has a pole, $s = -1/a.T_{eq}$. Hence, the system can be simplified as follows.

$$G_{v,CL}(s) = \frac{1 + a^2.T_{eq}.s}{(a.T_{eq}.s + 1).(a^2.T_{eq}{}^2.s^2 + a.(a-1).T_{eq}.s + 1)} \tag{3.51}$$

From the denominator of the transfer function Eqn.(3.51), the roots of the characteristic equation are,

$$s_1 = \frac{-1}{a.T_{eq}} \tag{3.52}$$

$$s_2, s_3 = -\left(\frac{a-1}{2.T_{eq}} \right) \pm \sqrt{\left(\frac{a-1}{2.a.T_{eq}} \right)^2 - \left(\frac{1}{a.T_{eq}} \right)^2} \tag{3.53}$$

This generalization shows three conditions for roots s_2,s_3: for a given value of T_{eq}, if '*a*' is varied, the roots start from complex conjugate roots on imaginary axis for *a*=1, and move away from imaginary axis, becoming real and equal at *a*=3 and if increased further, the roots move along the real axis becoming real and distinct, as shown in Fig.3.11.

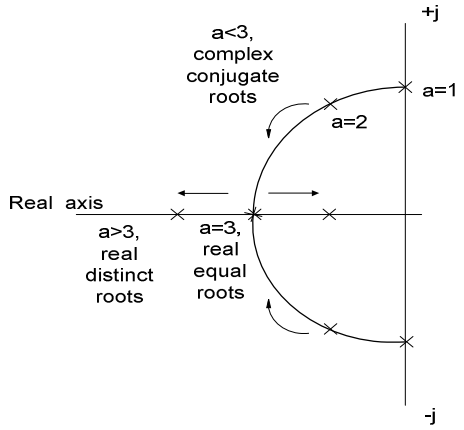

Figure 3.11 – Locus of roots s_2 and s_3 with variation in 'a'

In symmetric optimum tuning as in Section 3.4.3.1, the value of '*a*' is chosen for the condition fulfilling desired performance: the specifications could be the cross-over frequency at which the phase margin is maximum, or the value of desired phase margin. However, the specifications should result in the value of '*a*' in the acceptable region. Lower values of '*a*' give a small phase margin and high oscillations, while increasing values of '*a*' may lead to better damping but slower response.

Symmetrical optimum method can be extended so as to specify damping factor for the system as part of tuning procedure using pole placement [19]. For closed loop system Eqn.(3.51), if the real pole is located very far from the origin, transients corresponding to such remote pole are small, last for short time and can be neglected. The system can then be approximated by a second order system, for an easier estimate of response characteristics. But when specifying '*a*', there is no control over relative spacing of the real pole and the complex poles, so such a simplification and degree of freedom can not be achieved.

3.4.3.4 Tuning of dc-voltage controller using Pole placement

Using the symmetric optimum method, controllers can be tuned for variable damping by specifying the value of a, but the range of variation is very small, and when specifying 'a', there is no control over relative spacing of the real pole and the complex poles. Pole placement interpretation of symmetrical optimum method is a special case of symmetric optimum tuning, which considers $a<3$. That is, the characteristic equation has one real root, p and a pair of complex conjugate roots, $\sigma \pm j\omega$. The derivation of the tuning criteria is presented in Appendix-F. The tuning of controller parameters by pole placement in symmetric optimum method is given by,

$$K_{pv,pu} = \frac{1+2\alpha\zeta^2}{\zeta^2.(\alpha+2)^2}\frac{T_c}{KT_{eq}} \quad \text{and} \quad T_{iv} = \frac{T_{eq}(\alpha+2)(2\alpha\zeta^2+1)}{\alpha} \tag{3.54}$$

The resulting closed loop transfer function is then,

$$G_{V,CL}(s) = \frac{\alpha + (\alpha+2)(2\alpha\zeta^2+1)T_{eq}s)}{(\alpha+2)^3 T_{eq}{}^3\zeta^2 s^3 + (\alpha+2)^3 T_{eq}{}^2\zeta^2 s^2 + (\alpha+2)(2\alpha\zeta^2+1)T_{eq}s + \alpha} \tag{3.55}$$

3.4.4 Active and Reactive Power Controllers

Using the base system given in Appendix-B, the active and reactive power of the system in per unit can be written as,

$$\begin{aligned} p_{pu} &= v_{dpu}.i_{dpu} \\ q_{pu} &= -v_{dpu}.i_{qpu} \end{aligned} \tag{3.56}$$

The active and reactive power can thus be controlled in the simplest way using open loop controller. But more accurate control is achieved if a feedback loop is employed using PI controllers. The control loops of active and reactive power are shown in Fig.3.12 and 3.13. The block diagrams are derived considering the first order approximation of inner current controller.

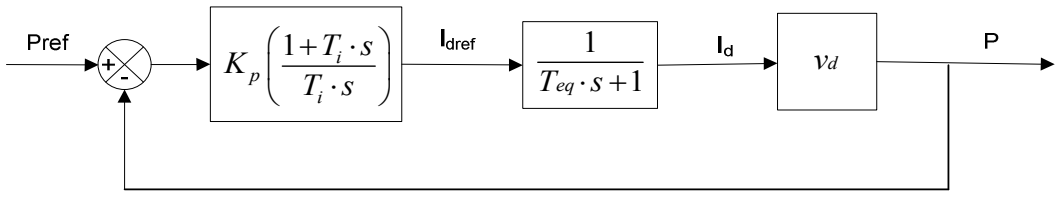

Figure 3.12 – Block diagram of active power control in per unit

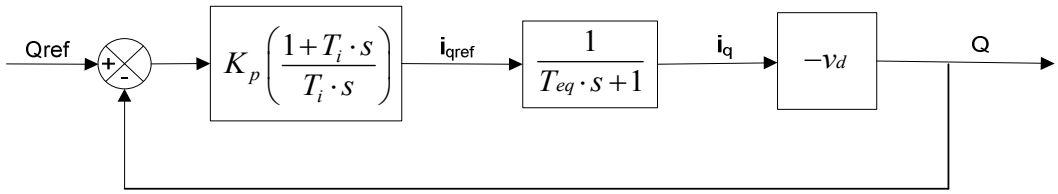

Figure 3.13 – Block diagram of reactive power control in per unit

The PI controllers in this case can again be tuned according to the symmetrical optimum method as applied to the dc voltage controller. The tuning criteria can be derived using description in Appendix-E. As the major focus in this thesis is on dc voltage controller, the tuning of active and reactive power controllers is not dealt in detail here.

Chapter 4

Simulation and Results

4.1 Test System

The system considered in this thesis is given in Fig.4.1. The HVDC system consists of two VSCs connected via a dc link. The control of converter VSC-1 is done by using dc-voltage control and reactive power control whereas the control of converter VSC-2 is done by active and reactive power control.

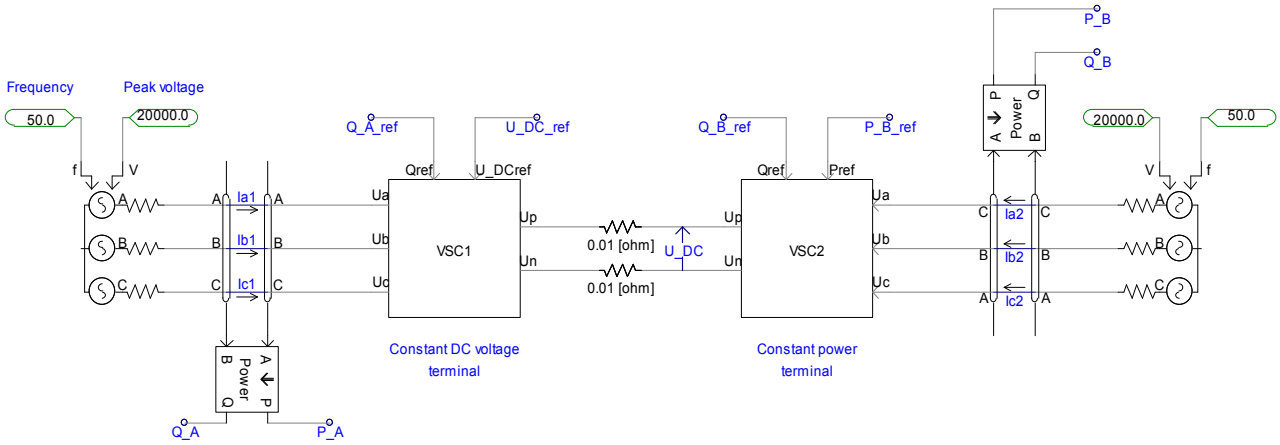

Figure 4.1 – Test System under consideration:- EMTDC/PSCAD

The system parameters are

Per unit inductance L_{pu} = 0.25133

Per unit capacitance, C_{pu}= 0.497359

Per unit resistance, R_{pu} = 0.066

Base frequency, ω_b = 314.1592

DC resistance = 0.01 Ω

The switching frequency of the converter block (f_{switch}) is taken as 5kHz. Average time delay of converter is then,

$$T_a = \frac{T_{switch}}{2} = \frac{1}{2 . f_{switch}} = 100\,\mu s$$

4.2 Transfer Function Analysis

4.2.1 Current Controller tuning by Modulus Optimum

The current controller was tuned using modulus optimum criteria as discussed in Section 3.3.3.2. The parameters and the transfer functions are given below.

Controller gain, $K_{p,pu} = \frac{\tau_{pu} \cdot R_{pu}}{2 \cdot T_a} = 4$

Integral time constant, $T_i = \tau_{pu} = \frac{L_{pu}}{\omega_b . R_{pu}} = 0.012$

Thus, $K_{i,pu} = \frac{K_{p,pu}}{T_i} = 333.33$

Substituting the values,

$$G_{C,OL}(s) = \frac{5000}{0.0001s^2 + s}$$

$$G_{C,CL}(s) = \frac{1}{20 \times 10^{-9} s^2 + 0.0002s + 1}$$

Where, $\omega_n = 7071 rad/s$ and $\zeta = 0.707$.

4.2.1.1 Frequency domain analysis

With the calculated open loop transfer function, the Bode plot is obtained for the system, as shown in Fig.4.2. The Bode plot shows a phase margin is 65.5° and gain margin is infinite. From the frequency domain stability criteria [20], the Bode plot shows the closed loop system to be stable. A sufficiently high phase margin shows that the system is robust.

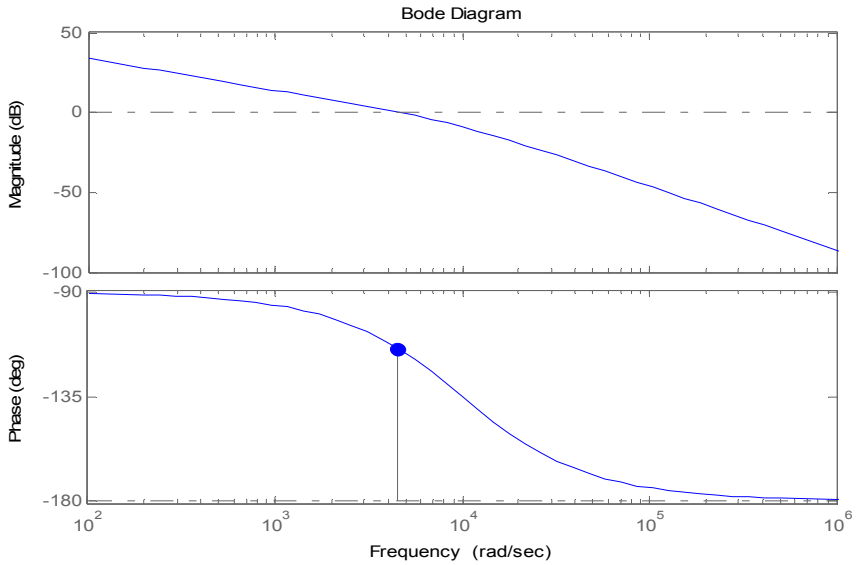

Figure 4.2 – Open loop Bode plot of current controller transfer function

4.2.1.2 Time domain analysis

The time domain analysis of the system was performed by exciting the system through a unit step function. The resulting response is shown in Fig.4.3. From the response to the step input function,

Maximum Overshoot, M = 1.04

Time for maximum overshoot, t_m = 0.0006s

Settling time, using 2%criteria, t_s = 0.0008s

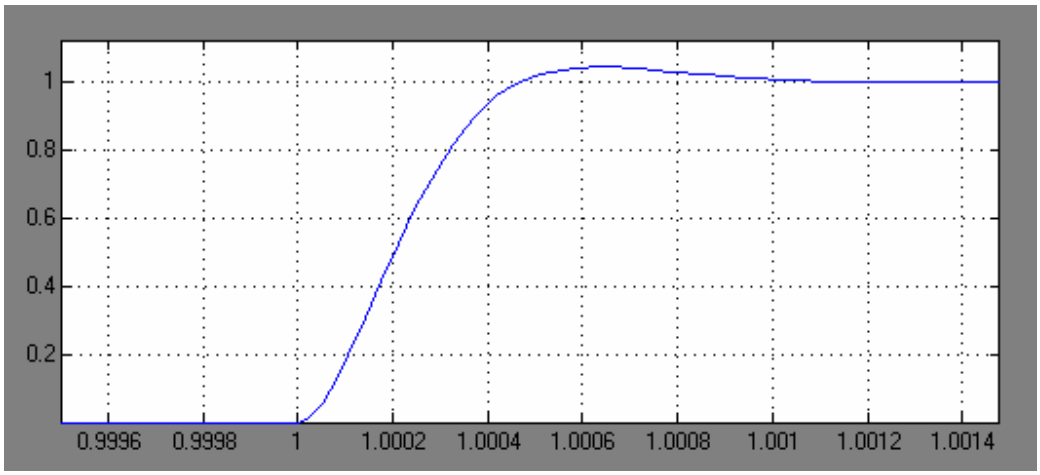

Figure 4.3 – Step response of Current controller tuned with modulus optimum

The time response to step function also shows that the response is very fast and with very small overshoot.

4.2.2 DC Voltage Controller Tuning by Symmetrical Optimum

The choice of controller parameters for dc voltage controller by using symmetrical optimum is done as discussed in Section 3.4.3.2. Most of the literature recommend the use of the criteria $T_{iv} = 4T_{eq}$ (a=2) for the Symmetrical optimum tuning [18]. The resulting performance gives an overshoot of around 43%, settling time around 16.3 T_{eq} and a phase margin of about 36°. The phase margin value is low and the system has a high overshoot. With higher values of a, the phase margin is increased and the overshoot also decreases, but the system response becomes slower. The recommended value of a is constrained between 2 and 4 in literature [19].

In this thesis, the tuning is done by choosing a=3. Thus,

$$T_{iv} = 9.T_{eq} \text{ and } K_{pv,pu} = \frac{T_c}{3.K.T_{eq}}$$

From the approximation of current control block, $T_{eq} = 2.T_a = 0.0002s$

For the steady state operating conditions, $V_{dpu} = V_{dcpu} = 1pu$. Thus K = 1.

Then applying the tuning rule to the per-unit system yields,

$$T_{iv} = 9.T_{eq} = 0.0018s$$

$$K_{pv,pu} = \frac{T_c}{3.T_{eq}} = 10.6667$$

Thus, $K_{iv,pu} = \frac{K_{pv,pu}}{T_{iv}} = 5925.94$

Now with the chosen control parameters, the open loop transfer function becomes,

$$G_{V,OL}(s) = \frac{0.0018s + 1}{2.16 \times 10^{-10}.s^3 + 1.08 \times 10^{-6}.s^2}$$

Which gives, the closed loop transfer function as,

$$G_{v,CL}(s) = \frac{0.0018s + 1}{2.16 \times 10^{-10}.s^3 + 1.08 \times 10^{-6}.s^2 + 0.0018s + 1}$$

4.2.2.1 Frequency domain analysis

With the calculated open loop transfer function, the Bode plot is obtained for the system, as shown in Fig.4.4. From the open loop transfer function, with chosen value of time constant of controller, the phase margin should be,

$$\Phi_M = \tan^{-1} 3 - \tan^{-1} \tfrac{1}{3} = 53.13^\circ \text{ at } \omega_d = 1/a.T_{eq} = 1666.67 rad/s$$

The open loop plot is as shown, which shows stable operating limits with a phase margin of 53.1° as calculated, which occurs at frequency 1.67e+3 rad/s. It is seen that for any chosen value of *a* (i.e. the ratio of controller time constant to small time constants), the phase margin reaches its maximum value at the crossover frequency, depending on the value of ratio chosen. Hence the tuning method ensures a maximum phase margin at designed frequency. The resulting transfer function behaves like a band pass filter as seen from the plot, and hence, the tuning of controller by symmetric method is effective for disturbance rejection.

However, the design of controller for dc voltage controller is done on the basis of linearization of system equations. Hence the stability of the controller is ensured by Bode plots is indeed locally stability around the operating point. But the linear analysis does not provide any information on the extent of the stability region.

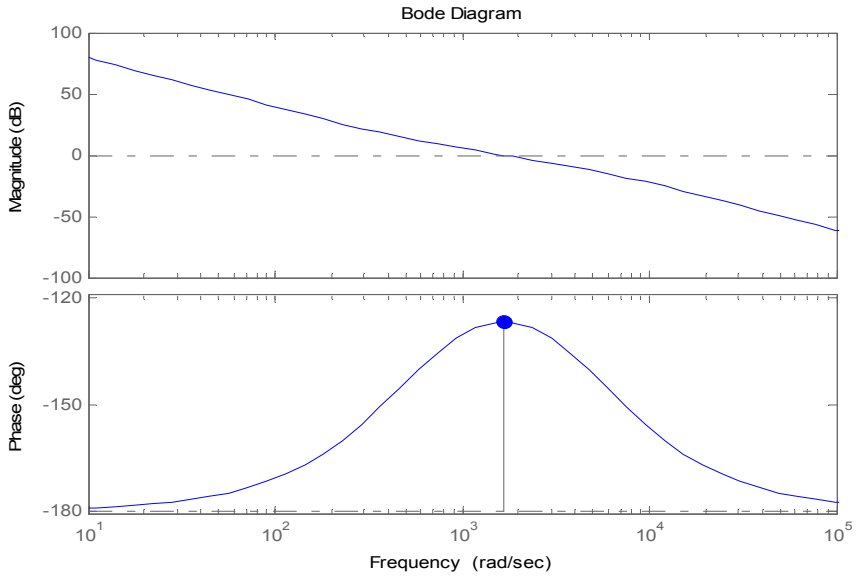

Figure 4.4 – Open loop Bode plot of dc voltage controller transfer function

4.2.2.2 Time domain analysis

The time domain analysis of the system was performed by exciting the system through a unit step function. The resulting response is shown in Fig.4.5. From the response to the step input function,

Maximum Overshoot, M = 1.25

Time for maximum overshoot, t_m = 0.00018s

Settling time, using 2%criteria, t_s = 0.0048s

The time response to step function shows that the system response is nearly six times slower than that of inner current controller and has a high overshoot.

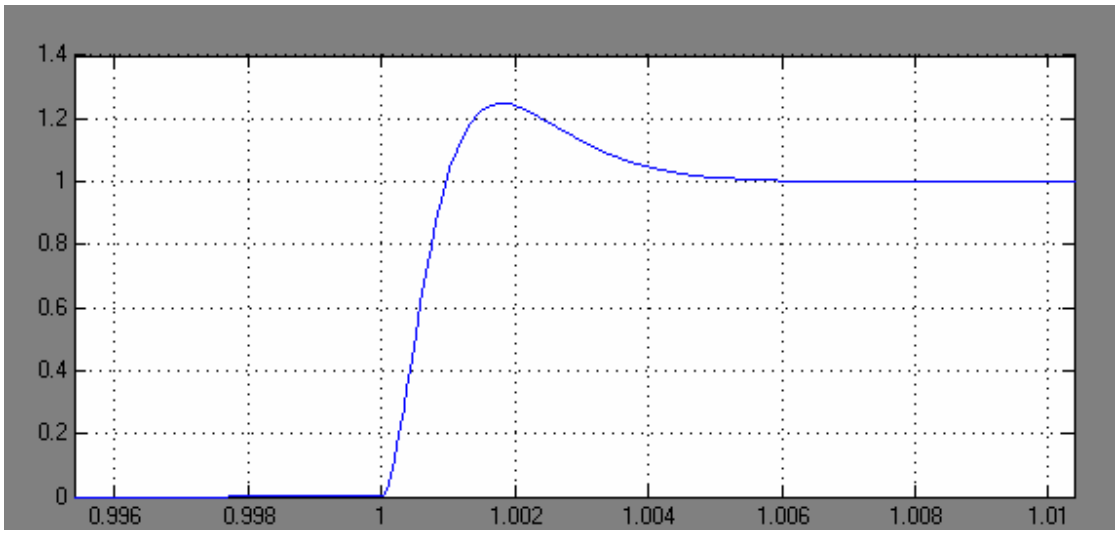

Figure 4.5 – Step response of dc voltage controller tuned with symmetric optimum

4.2.3 DC Voltage Controller Tuning by Pole Placement

Tuning voltage controller using pole placement is a special case of tuning using symmetric optimum, where the placement of the real pole and the damping of complex pole can be specified. For a particular case of α=10 and ζ=0.707, the controller parameters were tuned by pole placement resulting in,

Controller gain, $K_{pv,\,pu}$ = 4.888

Integral time constant, T_{iv} = 0.00264

Then the open loop transfer function reduces to

$$G_{V,OL}(s) = \frac{763.75s + 289299.24}{0.0002s^3 + s^2}$$

Which gives, the closed loop transfer function as,

$$G_{v,CL}(s) = \frac{763.75s + 289299.24}{0.0002s^3 + s^2 + 763.75s + 289299.24}$$

4.2.3.1 Frequency domain analysis

With the calculated open loop transfer function, the Bode plot is obtained for the system, as shown in Fig.4.6. The open loop plot shows stable operating limits with a phase margin of 56°.

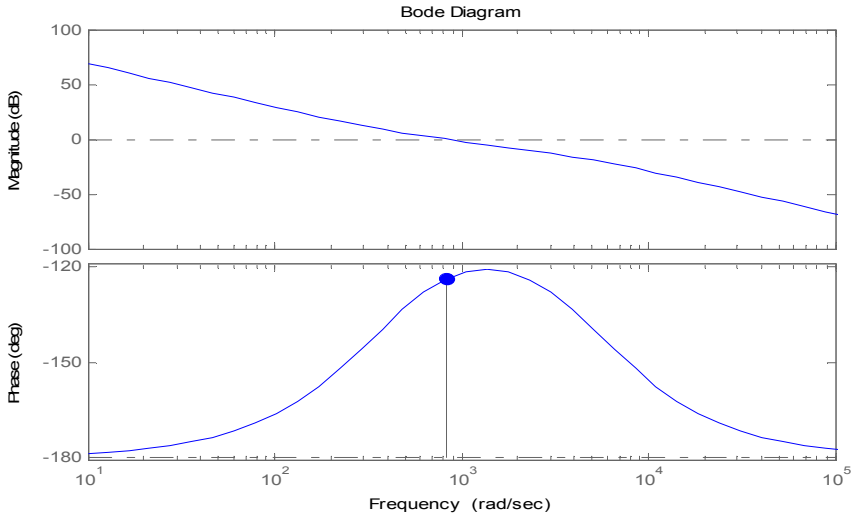

Figure 4.6 – Open loop Bode plot of dc voltage controller transfer function

4.2.3.2 Time domain analysis

There are two parameters α and ζ that can be specified for a desired performance and the variation of step response with these parameters are shown in Fig. 4.7 and 4.8. It is seen that by specifying the damping factor of the complex poles, the overshoot in the step response of third order system can be changed. With increasing ζ, the overshot is decreased and the speed of response is slightly decreased. On the other hand, for a given value of ζ increase in α seems to make the response slow with slight decrease in overshoot.

The time domain analysis of the system with α=10 and ζ=0.707 gives the following time response parameters.

Maximum Overshoot, M = 1.25

Time for maximum overshoot, $t_m = 0.004s$

Settling time, using 2%criteria, $t_s = 0.0086s$

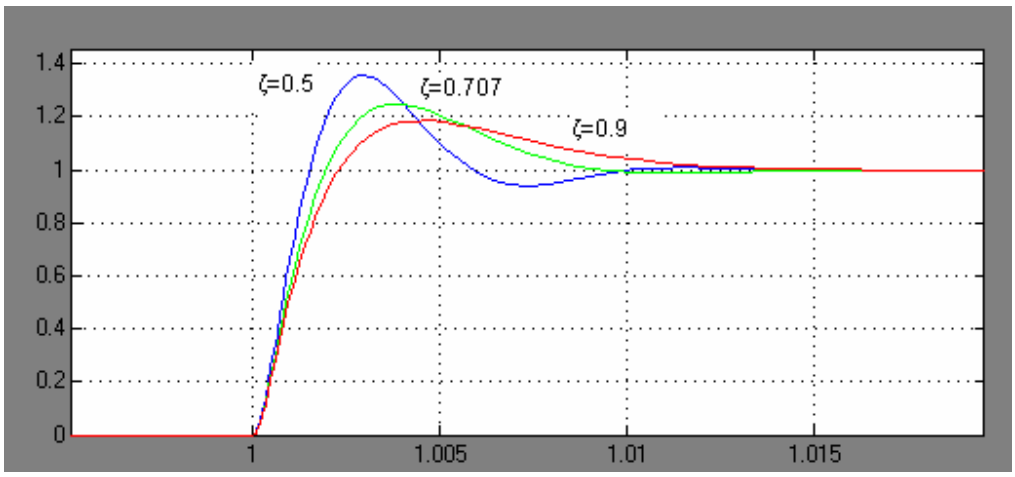

Figure 4.7 – Step response for fixed value of α=5, and varying ζ = 0.5, 0.707 and 0.9

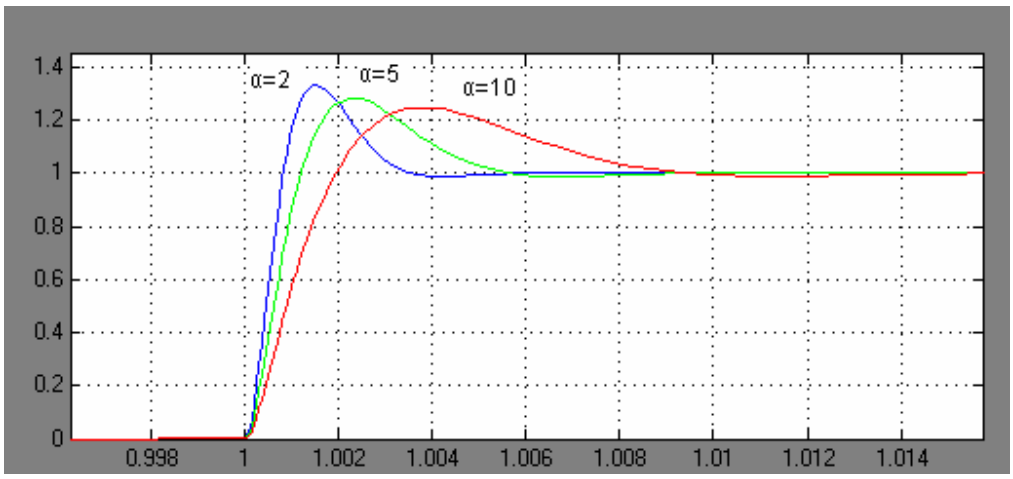

Figure 4.8 – Step response for fixed value of ζ =0.707, and varying α = 2, 5 and 10

With the specified value of α and ζ, the tuning of controllers using pole placement was found to result in a slower response.

4.3 Simulation Results

The simulation model in EMTDC/PSCAD as given in Fig.4.1 was tested for the controller performance under four different cases. In the PSCAD model, the direction of current is

considered from ac system to the converter and the power is considered positive when entering the converter. So load power drawn at converter-2 station is shown as positive. The test cases are presented as follows. All the test cases are plotted for time interval t = 0.1s to t = 0.8s.

4.3.1 Case 1: Transients in DC Voltage

For simulating the transients in dc voltage, the operating dc voltage was first set to 1pu. At t =0.3s, the dc voltage reference is increased to 1.5 pu and again reduced back to 1pu at t = 0.6s. The waveforms of dc voltage, active and reactive power at both terminals and the d and q components of current as well as load current seen by the sending end converter are plotted as given in Fig.4.9. The receiving end converter is controlled for a constant active power, so behaving as a constant power load. Reactive powers at both ends are set to be zero in this case.

It can be observed from the response of Fig.4.9 that change in dc voltage reference requires a change of current to maintain an active power balance. Hence we can see a change in load current maintaining the active power almost constant. However the change in references gives some transients in the active power as well, which is reflected in the d-component of current. It can be seen that the effect of transient is not present in the reactive power or q-component of current. Hence the decoupled control of active and reactive power is also ensured. The PI controller performs well in tracking the reference input.

The same case was repeated for the tuning of converters using tuning of dc voltage controller by pole placement method. The results were similar as of symmetrical optimum case, with slightly higher overshoot as shown in Fig.4.10. Hence for further cases, the system response with dc controller tuning with pole placement interpretation of symmetrical optimum is not carried out.

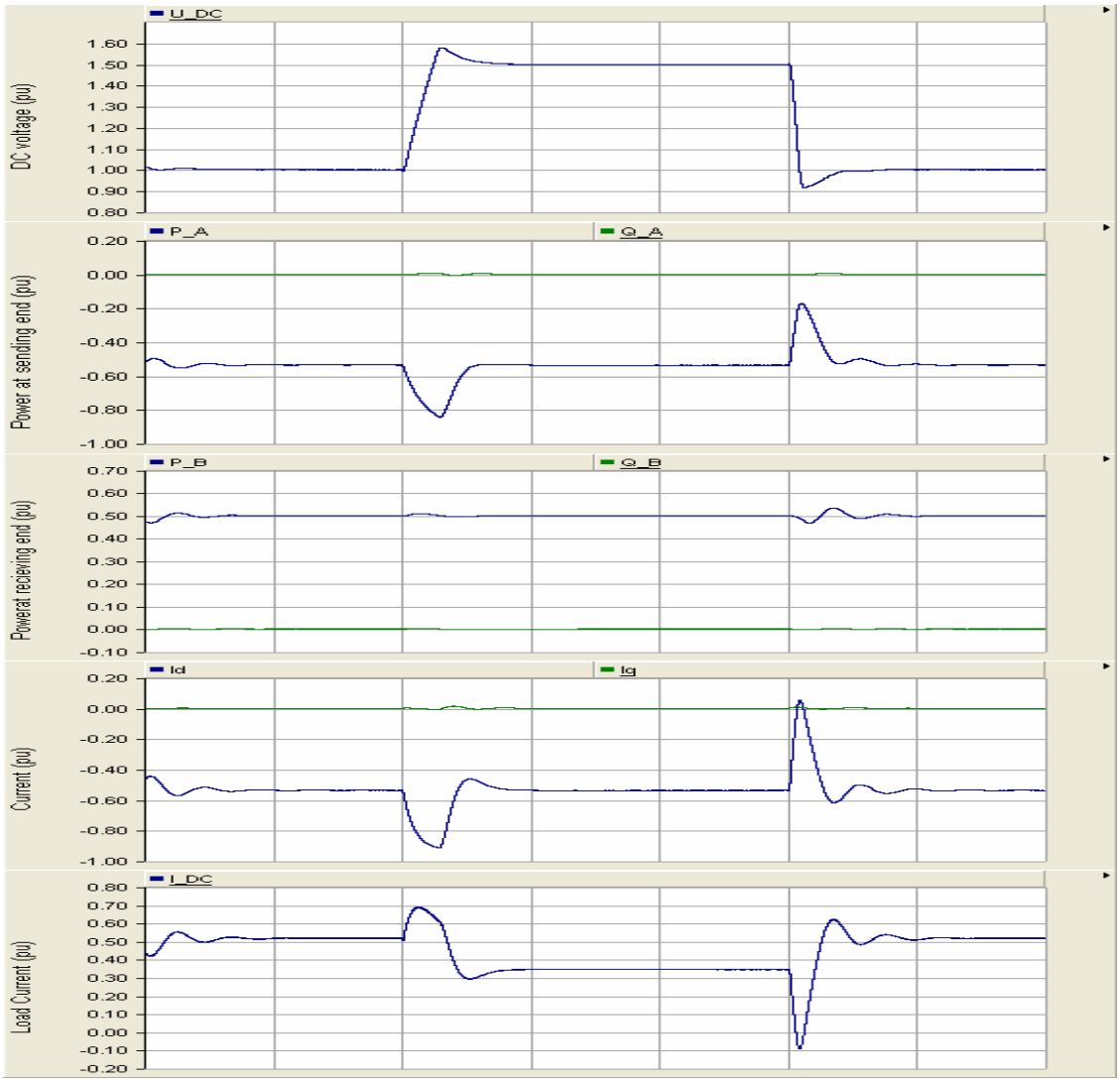

Figure 4.9 – Transient response for direct voltage reference changes

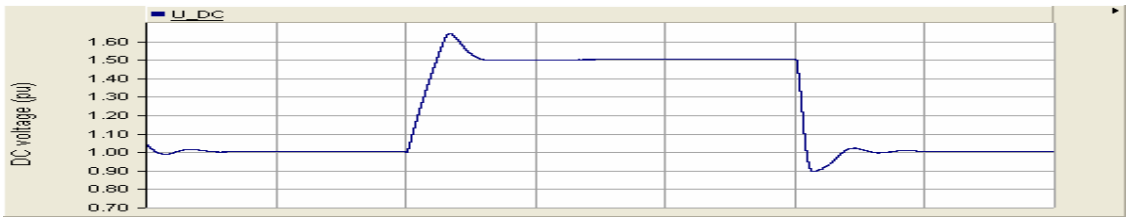

Figure 4.10 – Transient response for dc voltage reference change

4.3.2 Case 2: Change in reactive power

In this case, the dc voltage reference value is held at 1pu. The system is initially operating with a reactive power reference of 0.4pu and active power reference of 0.5pu. At t = 0.3s, the reactive power reference is reversed to 0.4pu at the sending end whereas the reference at the receiving end is retained at constant 0.4 pu. The responses of the system are shown in Fig.4.11.

It is seen that the system works well even in case of change of direction of reactive power flow. There is a very small ripple in dc voltage during the transient in reactive power, which is again reflected in the d-current reference. The active power is maintained at the reference value constantly, and hence is the load current seen from the sending end. The change in reactive power is reflected in the change of q-component of current, whereas the d-component remains constant, showing the decoupling of the d and q axis components.

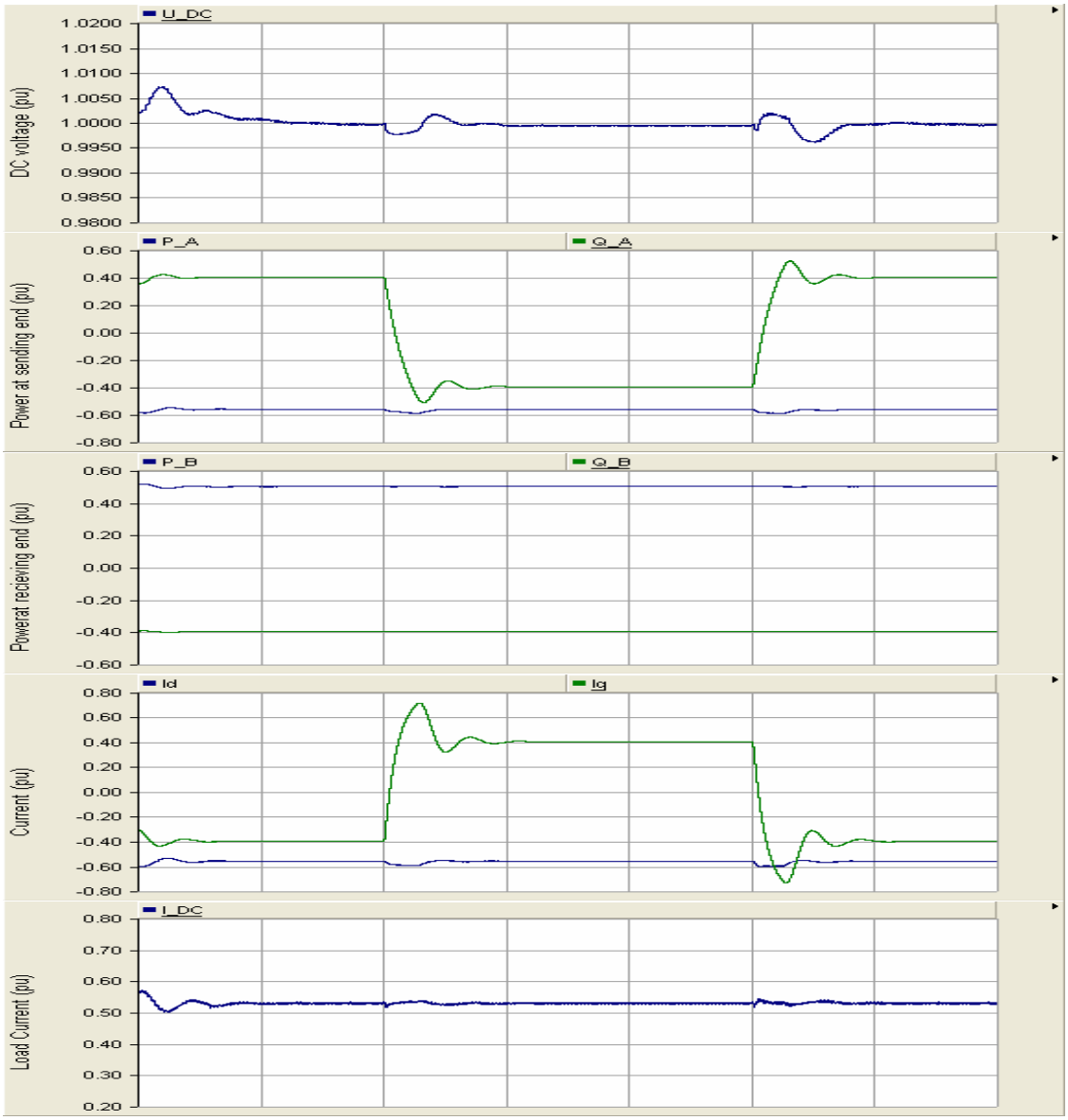

Figure 4.11 – Transient response for change in direction of reactive power at VSC-1

4.3.3 Case 3: Change in active power load

In this case, with the dc voltage reference set at 1pu, and the reactive power references set at 0.2pu and active power reference set at 0.5pu, the load at receiving end is changed from 0.5pu to -0.5pu.

From the responses plot in Fig.4.12, the system works stably with the reversal of active power as well. The change in active power is reflected in d-component of current and the load current magnitude and direction. Because of the decoupling, almost no effect is observed in the control of reactive power. The step change causes transients in dc voltage, but, the step change in active power causes a much higher transient than that with the change in reactive power.

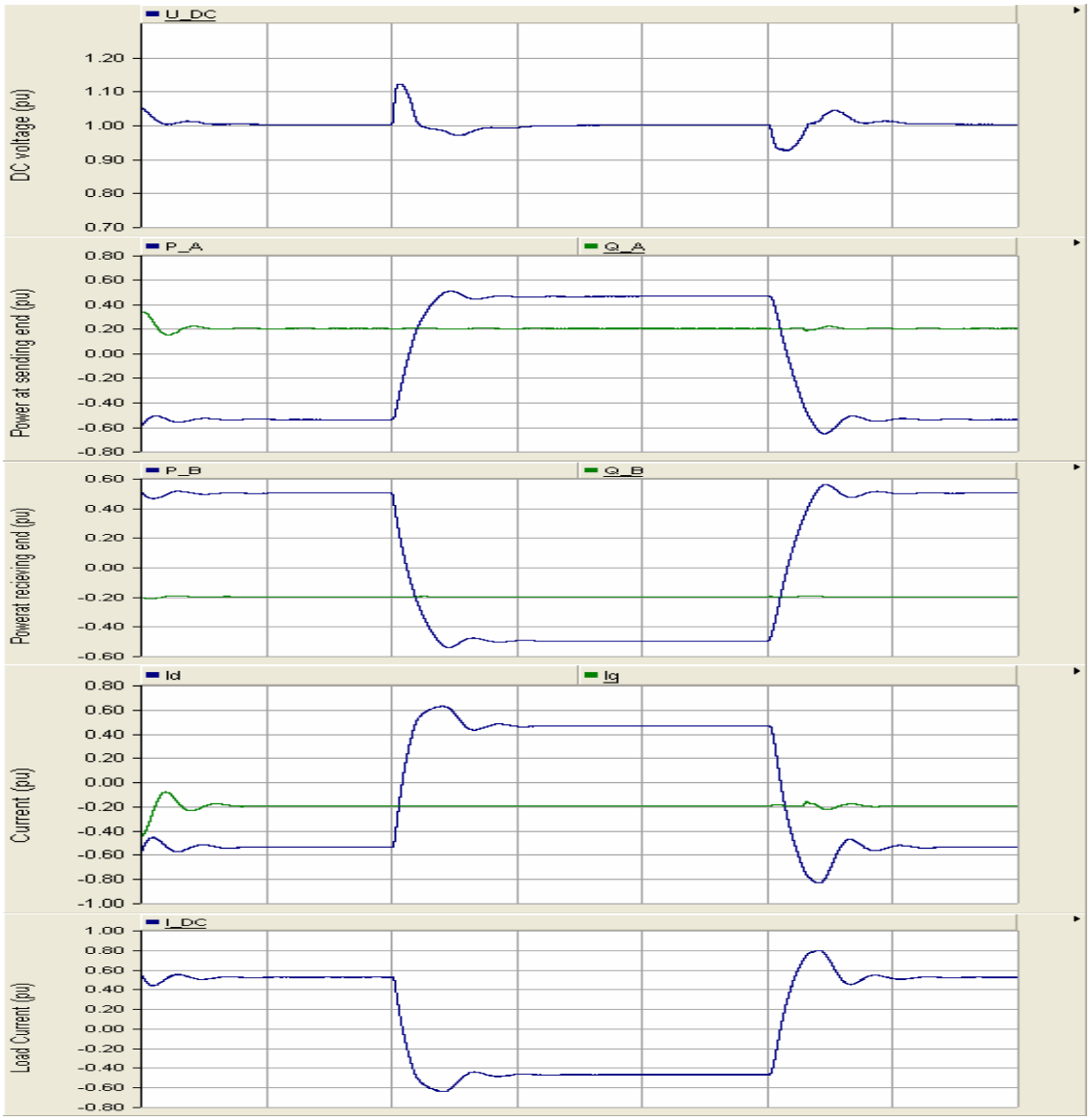

Figure 4.12 – Transient response for change in direction of active power at VSC-2

4.3.4 Case 4: Unbalance fault conditions

In this case, an unbalance fault is considered at the sending end of the HVDC link. The system is in balance condition with reference dc voltage at 1pu, reactive power references at 0.4pu and active power reference at 0.5pu. Unbalance fault is simulated through solid single line to ground fault near VSC-1 at t = 0.4. After 0.2s, the fault is removed and the system is back to normal operating conditions.

The response of the system under unbalance fault is shown in Fig.4.13. It is seen that under unbalance conditions, the control scheme produces distorted currents and the distortion of the dc voltage increases as well. During the fault, the ripples of double the system frequency (100Hz) appear at the dc voltage and there is a significant increase in reactive power. The d and q components of currents are also oscillating at 100Hz and no longer are decoupled constant dc quantities. The oscillation appears in dc load current as 50Hz oscillations.

It shows that the control scheme requires some adjustments for unbalance system operating conditions. The poor performance of the current controller in unbalanced conditions is due to the negative sequence component of grid voltage [21]. To eliminate dc link voltage ripple and dc component of reactive power, both positive and negative sequence of the currents need to be controlled simultaneously. The existence of positive and negative sequence components in the voltage and current allows the separation of the fundamental effective apparent power into positive-sequence power and a remaining component attributed to the system unbalance, thus enabling a modification of the control accordingly. The control method uses two synchronously rotating reference frames and two pairs of PI controllers situated in the reference frames rotating in opposite directions [21,22]. The same control strategy and tuning rules can be applied for the positive and negative sequence current controllers respectively.

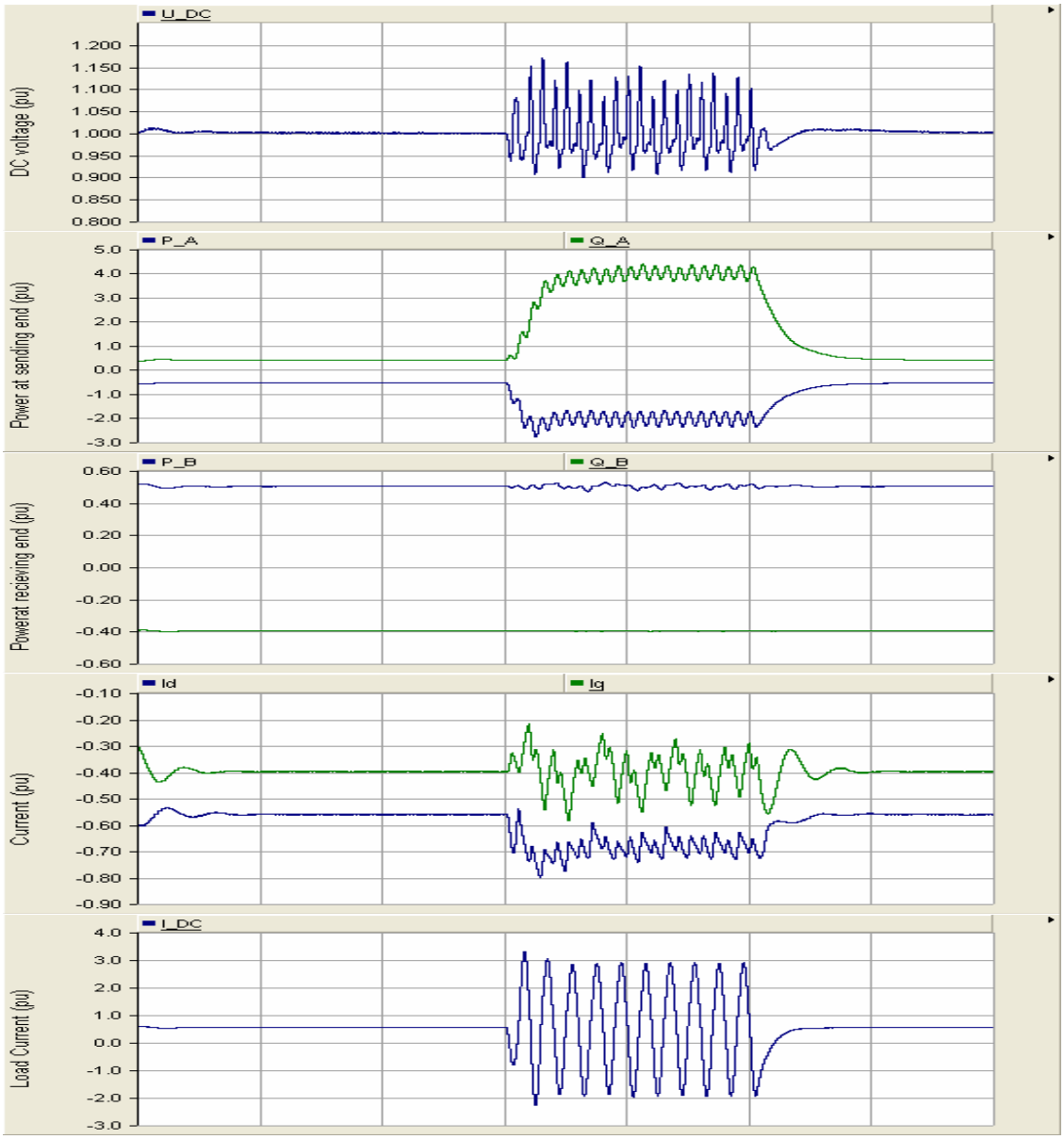

Figure 4.13 – Transient response for single phase to ground fault at VSC-1

Conclusion

A model of a VSC-HVDC system is presented in this thesis. The control strategy is described and implemented in PSCAD/EMTDC. Tuning rules for the converter controllers have been established and tested through simulations. The control system of the VSC-HVDC is based on a fast inner current control loop controlling the ac current in combination with a number of outer controllers. The thesis was more focused on dc-link voltage controller as an outer controller.

Based on the mathematical model of three phase VSC in synchronous reference frame, transfer function of inner and outer control loop is formed. Tuning methods are investigated for PI controller parameter setting. Method of modulus optimum is used to derive parameters of the inner current controller and symmetrical optimum to derive parameters of outer dc voltage controller. General guidelines for tuning the controllers are presented and then tested under simulations in PSCAD.

From the simulation results, it is concluded that the system response is fast; control accuracy can be achieved; and that the active power and the reactive power can be controlled independently and bi-directionally. It shows a very stiff DC link control which proves the robustness of the controller, but fast transient variations of the operating point of the converter will cause transients in the dc voltage. The current controller shows poor performance under unbalanced conditions. Further investigations of the control strategy and tuning rules are necessary for improvements in the controller performance. Moreover, the analysis in this thesis has been done in continuous time domain. For assessing the controller performance in real system, the analysis should be carried out in discrete time domain, as applied for digital controllers.

Future Work

A good understanding of control strategies, control system, their drawbacks and advantages in most general operating conditions is necessary to derive the most relevant option for control of any system. Though the thesis has tried to present the control strategy and the tuning criteria, further investigations are required for a good understanding of problems regarding the control of VSC based HVDC system. Some of the possible future works could be listed as follows.

- Improvement in the control system to reduce or eliminate the harmonics, specially the second order harmonics on the dc voltage in case of unbalanced faults
- Extension and study of the tuning rules for other types of outer controllers (Active power, reactive power and ac voltage controllers)
- Study the effect of linearization of the system equation, effect of dc system capacitance, ac filters and connection to weak ac system
- Verification of disturbance rejection performance
- Comparative study of different tuning rules
- Analyze the effect of bad tuning of controller parameters on system performance and stability limits, taking into account the complexity of complete transfer function when there are several PI controllers in cascade
- Verification of robustness of the controller through discrete time domain design and analysis

References

1. Lie Xu, Bjarne R Anderson, "Grid Connection of Large Offshore Wind Farms using HVDC", Research article on Wind Energy, 2006; 9:371-382
2. www.abb.com/hvdc
3. www.energy-portal.siemens.com/static/de/de/products_solutions/3846_kn03011203.html
4. Ned Mohan, Tore M. Undeland and W. P. Robbins, "Power Electronics: Converters, Applications and Design", John Wiley and Sons Inc., pp- 460-468.
5. "Its Time to Connect", Technical Description of HVDC Light Technology, ABB.
6. Bahrman M P, Johnson B K, "The ABCs of HVDC Transmission Technologies", IEEE Power and Energy Mag., Mar./Apr. 2007.
7. Costa Papadopoulas et al, "Interconnection of Greek islands with dispersed generation via HVDC Light technology", ABB
8. T. Noguchi et al, "Direct Power Control of PWM Converter without power source Voltage Sensors", IEEE transactions on Industry applications, Vol 34, No 3, May/June 1998, pp 473-479
9. Ruihua Song et al, "VSC based HVDC and its control strategy", IEEE/PES Trans. and Distrb. Conference and Exhibition, 2005.
10. Marta Molinas, Bjarne Naess, William Gullvik, Tore Undeland, "Robust Wind Turbine system against Voltage sag with induction generators interfaced to the grid by power electronic converters", IEEJ Trans. IA, Vol 126, No 7, 2006.
11. R Pena, J C Clare, G M Asher, "Doubly fed induction generator using back to back PWM converters and its application to variable speed wind energy generation", IEE Proc.-ElectrPower Appl., Vol 143, No 3, May 1996.
12. Ref. J. Svensson, "Synchronization methods for grid connected voltage source converters", IEE proc.-Gen. Transm. Distrb., vol 148, no 3, May 2001.
13. S.-K. Chung, "Phase-locked loop for grid-connected three-phase power conversion systems," Proc. Inst. Electr. Eng-Electron. Power Appl.,vol.147, no. 3, pp. 213–219, May 2000.
14. M. Liserre, "Innovative control techniques of power converters for industrial automation", PhD Thesis, Politecnico di Bari, Italy, Dec. 2001.

15. Â. J. J. Rezek, C. A. D. Coelho, J. M. E. Vicente, J. A. Cortez, P. R. Laurentino, "The Modulus Optimum (MO) Method Applied to Voltage Regulation Systems: Modeling, Tuning and Implementation", Proc. International Conference on Power System Transients, IPST'01, 24-28 June 2001, Rio de Janeiro, Brazil.
16. W. Leonhard, Introduction to Control Engineering and Linear control Systems, New Delhi, 1976.
17. O. Aydin, A. Akdag, P. Stefanutti, N. Hugo, "Optimum Controller Design for a Multilevel AC-DC Converter System", Proc. Of Twentieth Annual IEEE Applied Power Electronics Conference and Exposition, APEC 2005, 6-10 March 2005, Vol. 3, pp. 1660-1666
18. S. Preitl and R. E. Precup, "An Extension of Tuning Relations after symmetrical Optimum Method for PI and PID Controllers", Automatica Vol. 35, 1999, pp 1731-1736,
19. M. Machaba, M. Braae, "Explicit Damping Factor Specification in Symmetrical Optimum Tuning of PI Controllers", Proc. of First African Control Conference, 3-5 Des. Cape Town, South Africa, pp. 399-404
20. K. Ogata, Modern Control Engineering, Prentice Hall International
21. G Saccomando and J Svensson, "Transient Operation of Grid connected Voltage Source Converter under Unbalance Voltage Conditions", IEEE Industry App. Conference, 36th IAS Annual Meeting, Vol 4, pp 2419-2424, Sept-Oct 2001.
22. H. Song and K Nam, "Dual Current Control Scheme for PWM Converter under Unbalanced Input Voltage Conditions", IEEE Trans. on Industrial Electronics, Vol. 46, No. 5, Oct. 1999.

Appendix

Appendix A: Park and Clark Transformation

The summary of the transformations are presented as follows.

Transformation	Transforms	Matrix for transformation
Clark transformation	from abc to αβ	$\frac{2}{3}.\begin{pmatrix} 1 & -1/2 & -1/2 \\ 0 & \sqrt{3}/2 & -\sqrt{3}/2 \end{pmatrix}$
Inverse Clark transformation	from αβ to abc	$\begin{pmatrix} 1 & 0 \\ -1/2 & \sqrt{3}/2 \\ -1/2 & -\sqrt{3}/2 \end{pmatrix}$
Park transformation	from αβ to dq	$\begin{pmatrix} \cos\theta & \sin\theta \\ -\sin\theta & \cos\theta \end{pmatrix}$
Inverse Park transformation	from dq to αβ	$\begin{pmatrix} \cos\theta & -\sin\theta \\ \sin\theta & \cos\theta \end{pmatrix}$

Appendix B: Example of DQ transformation

In linear ac circuits in a sinusoidal steady state, all voltages and currents vary sinusoidally with time. For an example of transformation, a time varying signal in stationary three phase stationary reference system is considered as,

$$\begin{pmatrix} V\cos\theta \\ V\cos(\theta - 2\pi/3) \\ V\cos(\theta - 4\pi/3) \end{pmatrix}$$

The transformation to stationary α-β reference is,

$$\frac{2}{3}.\begin{pmatrix} 1 & -1/2 & -1/2 \\ 0 & \sqrt{3}/2 & -\sqrt{3}/2 \end{pmatrix}.\begin{pmatrix} V\cos\theta \\ V\cos(\theta - 2\pi/3) \\ V\cos(\theta - 4\pi/3) \end{pmatrix} = \frac{2}{3}.\begin{pmatrix} 3/2.V\cos\theta \\ 3/2.V\sin\theta \end{pmatrix}$$

And the transformation to d-q reference is,

$$\begin{pmatrix} \cos\theta & \sin\theta \\ -\sin\theta & \cos\theta \end{pmatrix} . \frac{2}{3} . \begin{pmatrix} 3/2 . V\cos\theta \\ 3/2 . V\sin\theta \end{pmatrix} = \begin{pmatrix} V \\ 0 \end{pmatrix}$$

Thus the quantities that are time varying with respect to stationary three phase reference frame become a constant vector in the synchronously rotating reference frame.

Appendix C: Base System for Per Unit Representation

The following base system is chosen for conversion of the system into Per Unit (p.u.) representation.

S_b = Nominal three-phase power of the ac-grid

V_b = Nominal peak phase voltage at the ac side [$V_{peak.ph}$]

$= \sqrt{\frac{2}{3}} . V_{LL,rms}$ where $V_{LL,rms}$ = Line to Line Root Mean Square Voltage

I_b = Nominal peak phase current

$= \frac{2}{3} . \frac{S_b}{V_b}$

Z_b = Base ac impedance= $\frac{V_b}{I_b}$

ω_b = Base frequency

The base for per unit transformation is chosen as to achieve a power invariant transformation, so that the ac and dc side power is the same.

As, $S_{3phase} = 3 \cdot V_{phase} \cdot I_{phase}$ and then the power balance gives,

$$S_b = \frac{3}{2} \cdot V_b \cdot I_b = V_{dcbase} \cdot I_{dcbase}$$

The current cannot be controlled linearly when the voltage reference vector lies in over-modulation region. For the control system implementations to achieve low output current distortion, the dc voltage should be high enough, preventing saturation of current controller. The minimum value of required dc side voltage [11] is given by the inverter output voltage as,

$V_{dc} = 2.\sqrt{2/3}.V_{LL,rms} = 2.V_{peak,\,ph}$.

Hence the base value for dc voltage is chosen as,

$$V_{dcbase} = 2.V_{peak,ph} = 2.V_b,$$

Then by the power balance equation as above,

$$I_{dcbase} = \frac{3}{4}.I_b$$

And, Z_{dcbase} = Base dc impedance $= \frac{V_{dcbase}}{I_{dcbase}} = \frac{8}{3}.Z_b$

Appendix D: Representation of second order closed loop transfer function of inner current controller by equivalent first order function

The closed loop second order transfer function of current controller is given by,

$$W(s) = \frac{1}{2T_a{}^2 s^2 + 2T_a \cdot s + 1}$$

Let the transfer function be approximated by equivalent first order transfer function,

$$W'(s) = \frac{1}{T_{eq} \cdot s + 1}$$

The equivalent time constant T_{eq} of the approximated transfer function is evaluated by equating the error function of the two transfer functions.

Taking a step function $U(s) = \frac{1}{s}$ as an input,

The respective error functions of two transfer functions are given as,

$$Err_1(s) = \frac{1}{s} - \left(\frac{1}{s}.\frac{1}{2T_a{}^2 s^2 + 2T_a \cdot s + 1}\right) = \frac{2T_a{}^2 s + 2T_a}{2T_a{}^2 s^2 + 2T_a \cdot s + 1}$$

$$Err_2(s) = \frac{1}{s} - \left(\frac{1}{s}.\frac{1}{T_{eq} \cdot s + 1}\right) = \frac{T_{eq}}{T_{eq} \cdot s + 1}$$

And the condition for the two transfer functions to be equal is,

$$\int_0^\infty Err_1(t).dt = \int_0^\infty Err_2(t).dt$$

By definition of Laplace transform, we have,

$$L\left[Err_1(t)\right] = Err_1(s) = \int_0^{\infty} e^{-st}.Err_1(t).dt$$

Taking limit $s \to 0$, the equation then becomes,

$$\lim_{s\to 0} Err_1(s) = \int_0^{\infty} Err_1(t).dt$$

Hence the equality condition becomes,

$$\lim_{s\to 0} Err_1(s) = \lim_{s\to 0} Err_2(s)$$

$$\lim_{s\to 0} \frac{2T_a{}^2 s + 2T_a}{2T_a{}^2 s^2 + 2T_a \cdot s + 1} = \lim_{s\to 0} \frac{T_{eq}}{T_{eq} \cdot s + 1}$$

Thus, $2T_a = T_{eq}$

Appendix E: Derivation of Tuning Criteria using Symmetric Optimum condition

Given open loop transfer function,

$$G_{V,OL}(s) = K_{pv,pu} \cdot \left(\frac{1 + T_{iv} \cdot s}{T_{iv} \cdot s} \right) \cdot \frac{K}{1 + T_{eq} \cdot s} \cdot \left(\frac{1}{s \cdot T_c} \right)$$

The transfer function in frequency domain can be written as,

$$G_{V,OL}(j\omega) = \frac{K_{pv,pu}.K}{T_c.T_{iv} \cdot (j\omega)^2} \cdot \left(\frac{1 + T_{iv} \cdot (j\omega)}{1 + T_{eq} \cdot (j\omega)} \right)$$

The Nyquist criteria of stability is,

$\left|G_{V,OL}(j\omega)\right| = 1$ and

$\measuredangle G_{V,OL}(j\omega) = -180^\circ + \Phi_M$, where Φ_M is the phase margin.

We have from the open loop transfer function,

$$\measuredangle G_{V,OL}(j\omega) = -180^\circ + \tan^{-1}(\omega T_{iv}) - \tan^{-1}(\omega T_{eq}) = -180^\circ + \varphi$$

The angle φ is positive for all values of ω. Differentiation of this angle with respect to ω can give the maximum value of phase margin. The value of T_{iv} should be designed to be small, especially when φ approaches Φ_M, otherwise the response to the disturbances becomes slow.

From the maximization condition $\frac{d\varphi}{d\omega} = 0$, the angle is maximum when $\omega_d = \frac{1}{\sqrt{T_{iv}.T_{eq}}}$

Hence the phase margin,

$$\Phi_M = \tan^{-1}\sqrt{T_{iv}/T_{eq}} - \tan^{-1}\sqrt{T_{eq}/T_{iv}}$$

This condition gives the tuning criteria for time constant of the controller as,

$$T_{iv} = T_{eq}\cdot\left(\frac{1+\sin\Phi_M}{1-\sin\Phi_M}\right)$$

The resulting open loop frequency characteristic will have a maximum phase Φ_M at the crossover frequency of ω_d, symmetric about 1/ T_i and 1/T_{eq}. Then by symmetric property, we can also write,

$$T_{iv} = a^2.T_{eq}$$

where 'a' is the symmetrical distance between 1/ T_{iv} to ω_d, and 1/ T_{eq} to ω_d.

Again from the magnitude condition, the tuning for gain of controller can be found as follows.

$$\left|G_{V,OL}(j\omega)\right| = \frac{K_{pv,pu}.K}{\omega_d{}^2.T_{iv}.T_c}.\sqrt{\frac{(\omega_d T_{iv})^2+1}{(\omega_d T_{eq})^2+1}} = 1$$

That is, $K_{pv,pu} = \frac{T_c}{K.\sqrt{T_{iv}.T_{eq}}}$.

Appendix F: Derivation of Tuning Criteria using pole placement in Symmetric Optimum condition

Given open loop transfer function,

$$G_{V,OL}(s) = K_{pv,pu}\cdot\left(\frac{1+T_{iv}\cdot s}{T_{iv}\cdot s}\right)\cdot\frac{K}{1+T_{eq}\cdot s}\cdot\left(\frac{1}{s\cdot T_c}\right)$$

The closed loop transfer function based on this is given by,

$$G_{V,CL}(s) = \frac{\frac{K.K_{pv,pu}}{T_{iv}T_cT_{eq}} \cdot (1 + T_{iv} \cdot s)}{s^3 + \frac{1}{T_{eq}}.s^2 + \frac{K.K_{pv,pu}}{T_cT_{eq}}.s + \frac{K.K_{pv,pu}}{T_{iv}T_cT_{eq}}}$$

In symmetrical optimum tuning, when a<3, the characteristic equation has one real root, p and a pair of complex conjugate roots, $\sigma \pm j\omega$. Then it results in a characteristic equation as follows,

$$s^3 + (p+2\sigma).s^2 + (2p\sigma + \sigma^2 + \omega^2).s + p.(\sigma^2 + \omega^2)$$

The real pole placement is defined through a relation,

$p = \alpha.\sigma$ where α >1.

For the complex roots, the relation between damping factor and the roots is given by,

$$\omega^2 = \frac{1 - \zeta^2}{\zeta^2}.\sigma^2$$

Substituting the relations, the characteristic equation becomes,

$$s^3 + (\alpha+2).\sigma.s^2 + \left(2\alpha + 1 + \frac{1-\zeta^2}{\zeta^2}\right).\sigma^2.s + \left(1 + \frac{1-\zeta^2}{\zeta^2}\right).\alpha.\sigma^3$$

Comparing the characteristic equation with the one from original closed loop transfer function, gives,

$$(\alpha+2).\sigma = \frac{1}{T_{eq}}$$

$$\left(2\alpha + 1 + \frac{1-\zeta^2}{\zeta^2}\right).\sigma^2 = \frac{K.K_{pv,pu}}{T_cT_{eq}}$$

$$\left(1 + \frac{1-\zeta^2}{\zeta^2}\right).\alpha.\sigma^3 = \frac{K.K_{pv,pu}}{T_{iv}T_cT_{eq}}$$

From these relations, the controller parameters can be found in terms of α and ζ, as follows.

$$K_{pv,pu} = \frac{1 + 2\alpha\zeta^2}{\zeta^2.(\alpha+2)^2}\frac{T_c}{KT_{eq}}$$

$$T_{iv} = \frac{T_{eq}(\alpha+2)(2\alpha\zeta^2+1)}{\alpha}$$

Appendix G: Paper presented in NORPIE-2008, June 9-11, Helsinki

Part of the thesis was presented as a paper at NORPIE-2008.

Understanding of tuning techniques of converter controllers for VSC-HVDC

Chandra Bajracharya, Marta Molinas, Jon Are Suul, Tore M Undeland

***Abstract*— A mathematical model of a voltage source converter is presented in the synchronous reference frame for investigating VSC-HVDC for transferring wind power through a long distance. This model is used to analyze voltage and current control loops for the VSC and study their dynamics. Vector control is used for decoupled control of active and reactive power and the transfer functions are derived for the control loops. In investigating the operating conditions for HVDC systems, the tuning of controllers is one of the critical stages of the design of control loops. Three tuning techniques are discussed in the paper and analytical expressions are derived for calculating the parameters of the current and voltage controllers. The tuning criteria are discussed and simulations are used to test the performance of such tuning techniques.**

***Index Terms*—Voltage source converter; VSC-HVDC; Vector control; PI controller tuning; modulus optimum; symmetric optimum**

I. INTRODUCTION

NORTH of Norway has extremely good conditions for establishment of wind power generation farms, with a possibility of about 4000MW of wind power generation in this area. The main grid in Northern Norway consists of a weak 132 kV network, and considering the integration of massive amounts of wind power, the existing transmission lines, will not be able to handle and export the surplus energy from these areas to the consumption areas in the middle of Norway. Alternative methods are being considered for the integration of this new energy into the existing system. One of the alternatives is to build a new corridor with multi-terminal HVDC from Northern Norway to Middle of Norway. VSC-HVDC, the HVDC technology based on voltage source converters (VSC), has recently been an area of growing interest due to a number of factors: its modularity, independence of ac network, independent control of active and reactive power, low power operation and ability of power reversal etc [1]. VSC-HVDC technology has been promoted under the commercial trade names HVDC Light [2] and HVDC Plus (the "plus" stands for Power Link Universal Systems) [3]-[4] by two prominent manufacturers.

C. Bajracharya is with Norwegian University of Science and Technology, O.S. Bragstads plass 2E, 7491 Trondheim, Norway (47-7359-4237; fax: 47-7359-4279; e-mail: chandrb@stud.ntnu.no).

M. Molinas, J. A. Suul and T. Undeland are with Norwegian University of Science and technology (e-mail: marta.molinas@elkraft.ntnu.no, jon.are.suul@elkraft.ntnu.no, tore.undeland@elkraft.ntnu.no).

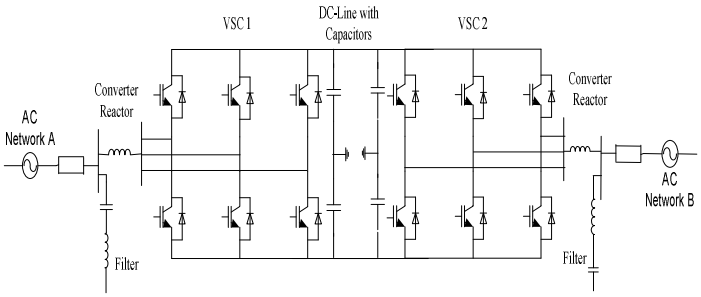

Fig. 1. VSC based HVDC link

As shown in Fig.1, a VSC based HVDC link consists of VSCs connected back to back via a dc-link. For analysis of the complete VSC-HVDC system, this paper starts from developing an understanding of a VSC from the control point of view. The control strategy used is based on field oriented vector control [5] of voltage source current controlled converters.

The VSC-HVDC operating characteristics are determined by the controllers including the system. Adequate performance of VSC-HVDC system under diverse operating conditions depends on the selection of robust parameters for the control system. Usually, due to the simple structure and robustness, PI controllers have been used to adjust the system for desired responses. The tuning of the converter controller parameters (gain and time constant) is a compromise between speed of response and stability for small disturbances as well as the robustness to tolerate large signal disturbances. Furthermore, the control loops are nonlinear in nature, and hence needs careful selection of control parameters to accommodate a range of operating conditions. Tuning rules should also take into account the effects of non-ideal operating conditions and try to minimise them.

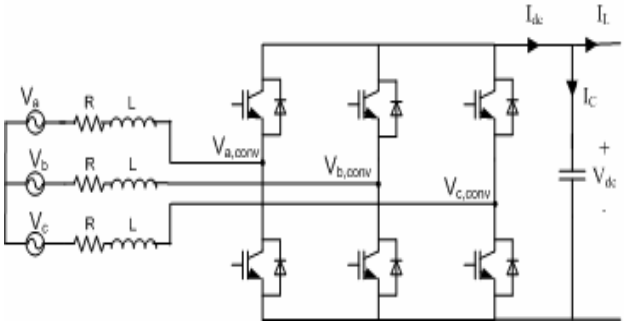

Fig. 2. Three phase PWM-VSC connected to ac source

In addition to the effects of controller tuning on the performance of the VSC-HVDC, it is claimed in [6] that design of converter control systems has an impact on sub-synchronous torque interaction. There exists certain parameter region of the converter controllers where unstable shaft torsional oscillations between the VSC-HVDC transmission link and a nearby generator may be caused. It is also claimed that with proper control parameter settings, no sub-synchronous damping control is needed.

This paper focuses on the control structure and tuning of the voltage source converter. The decoupled control of real and reactive power exchanged between the converter and the electric power system is explained. Analytical expressions, transfer functions and the tuning rules for the PI controllers are presented and discussed in an attempt to establish the criteria for tuning.

II. System Description

Fig.2 shows a schematic diagram of an ac source/grid connected to a PWM-voltage source inverter. The control of the converter aims at regulating the dc voltage V_{dc} and maintaining the balance between the dc link power and ac power supply. For that, standard field oriented vector control technique is implemented which gives decoupled control of active and reactive power [7].

For the analysis of the system, basic equations describing the system behavior are presented based on analysis done in [8]-[10]. The phase voltages and currents are given by the equation ,

$$V_{abc} = R.i_{abc} + L\frac{d}{dt}i_{abc} + V_{abc,conv} \quad (1)$$

where V_{abc}, i_{abc}, $V_{abc,conv}$ are ac voltages, currents and converter input voltages respectively and R and L resistance and filter inductance between the converter and the ac system.

The converter 3-phase currents and voltages are expressed in 2-axis d-q reference frame, synchronously rotating at given ac frequency, ω. The voltage equations in d-q synchronous reference frame are,

$$\begin{aligned} L\frac{di_d}{dt} &= -R.i_d + \omega L.i_q - V_{dconv} + V_d \\ L\frac{di_q}{dt} &= -R.i_q - \omega L.i_d - V_{qconv} + V_q \end{aligned} \quad (2)$$

The power balance relationship between the ac input and dc output is given as,

$$p = \frac{3}{2}(v_d.i_d + v_q.i_q) = v_{dc}.i_{dc} \quad (3)$$

where v_{dc} and i_{dc} are dc output voltage and current respectively. On the output side,

$$i_{dc} = C.\frac{dv_{dc}}{dt} + i_L \quad (4)$$

The d-axis of the rotating reference frame (Park's) is aligned to the ac voltage vector so that $v_q = 0$. With this alignment, the instantaneous real and reactive power injected into or absorbed from ac system is given by,

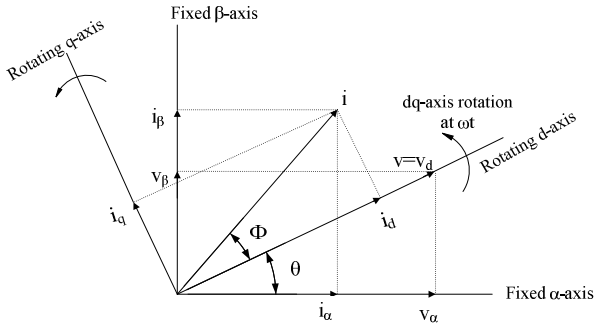

Fig. 3. Transformation of axes (α-β to d-q) for vector control

$$\begin{aligned} p &= \frac{3}{2}.v_d.i_d \\ q &= \frac{3}{2}.v_d.i_q \end{aligned} \quad (5)$$

Therefore, the control of active and reactive power reduces to the control of d and q components of current. The angular position of the voltage vector is given by,

$$\theta = \tan^{-1}\left(\frac{v_\beta}{v_\alpha}\right) \quad (6)$$

where v_α and v_β are components of voltage in stationary two axis reference frame (Clark's). The angle θ is computed using a phase lock loop (PLL) technique [11]-[12].

III. Presentation of the Control Scheme

The control scheme for the three-phase voltage source inverter is considered as cascade of two independent controllers, a dc voltage controller providing reference signals to the control system and the current controller that generates the switching signals according to the reference and measured signals, as shown in Fig 4.

A. Current Controller

As the currents are transformed to the synchronous reference frame, they become dc signals under balanced sinusoidal conditions and perfect synchronization [13]. Then PI controllers will ensure zero steady state error and increased robustness of the closed loop system.

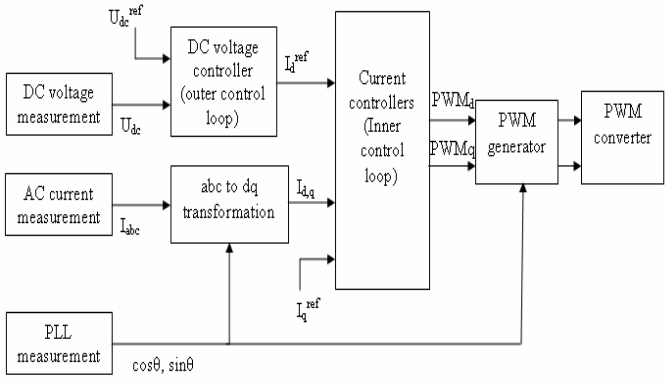

Fig. 4. Functional control diagram of VSC using vector control

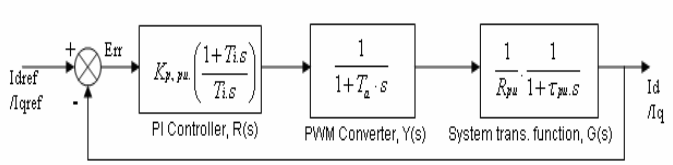

Fig. 5. Block diagram of PI Current control scheme in per unit

The control system requires a decoupled control of i_d and i_q. However, the model in synchronous frame (2) shows that the two axes are coupled due to the cross terms $\omega L.i_q$ and $\omega L.i_d$. When the cross coupling terms are compensated by feed-forward, the d-axis and q-axis components of currents can be controlled independently. Synchronous reference frame PI regulators then regulate the d and q components of currents. The two independent control loops in per unit system can be obtained [14] to be as shown in Fig. 5, where $K_{p,pu}$ and T_i are PI controller parameters, T_a is the delay caused by VSC switches and τ_{pu} is the per unit time constant of the line.

B. DC-link Voltage Controller

The current controller as described earlier ensures that the output current tracks the reference values generated by an additional external control loop, which performs the output active power regulation by implementing control of dc voltage. From (3)-(5), the dc link dynamics is given by,

$$C \cdot \frac{dV_{dc}}{dt} = \frac{3}{2} \cdot \frac{V_d}{V_{dc}} \cdot I_d - I_L \quad (7)$$

The minimum value of required dc side voltage [15] is given by the inverter output voltage as,

$$V_{dc} = 2 \cdot \sqrt{\frac{2}{3}} \cdot V_{LL,rms} = 2 \cdot V_{peak,\,ph} \quad (8)$$

where $V_{peak.ph}$ is peak phase voltage at the ac side and $V_{LL,rms}$ is the line-line rms voltage.

The dc-link dynamics, (7) is a non-linear equation and the parameters for the PI regulator need to be selected using linearization of system model around the operating point. The reference point for linearization is found by specifying reference input (V_{dcref}) for the nonlinear model. The linearization yields the transfer function as [14],

$$\frac{\Delta V_{dc}(s)}{\Delta i_d(s)} = \frac{3}{2} \cdot \frac{V_{d,0}}{V_{dc,ref}} \cdot \frac{1}{s.C} \quad (9)$$

For the analysis of the outer dc voltage control loop, the second order closed loop transfer function of the inner current controller is approximated by equivalent first order transfer function by equating the error functions of two transfer functions, which gives the equivalent time constant, T_{eq} to be $2T_a$ [14].

C. Feedforward in DC-link controller

Although simple to design and implement, a cascade control system is likely to respond to changes more slowly than a control system where all the system variables are processed and acted upon simultaneously [16]. The feed-forward is used to minimize disadvantage of slow dynamic response of cascade control.

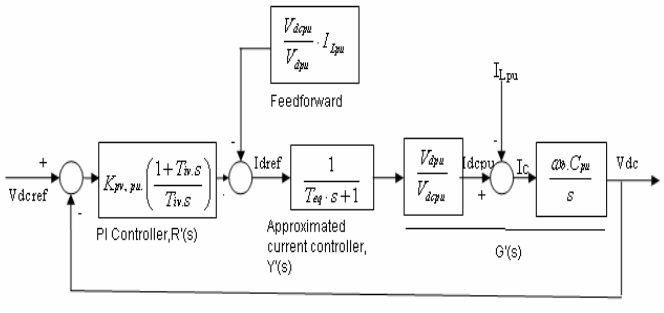

Fig. 6. Block diagram of dc-link voltage control scheme in pu

Using feed-forward, the load variation can be greatly reduced and the large gain of voltage controller otherwise required to reduce the large error is not necessary, which is important from stability viewpoint.

The dc link voltage controller controls the capacitor current so as to maintain the power balance. Hence under balanced conditions, i_c =0. That is, $I_{dc} = I_L$.
Thus, the reference value of I_d should be,

$$I_d = \frac{2}{3} \cdot \frac{V_{dc}}{V_d} \cdot I_L \quad (10)$$

which is the feed-forward term, ensuring exact compensation for load variation.

When the system equations are analysed in per unit [14], the complete block diagram of dc-link voltage controller can be represented as in Fig.6, where $K_{pv,pu}$ and T_{iv} are PI controller parameters, T_{eq} is the equivalent time constant of first order approximation of current control loop, and C_{pu} is per unit capacitance of dc link.

IV. Tuning of PI Controllers

In the tuning process of PI controllers, the nonlinearities are generally neglected, and tuning is done following the criteria adopted for electric drives [17]. Cascade control requires the speed of response to increase towards the inner loop. Hence, internal loop is designed to achieve fast response. On the other hand, main goal of outer loop are optimum regulation and stability. The inner loop is tuned according to "modulus optimum" condition because of fast response and simplicity whereas the outer loop according to "symmetrical optimum" condition for optimizing system behavior with respect to disturbance signals [18].

A. Modulus Optimum

For low order controlled plants without time delay the modulus optimum (absolute value optimum criterion) is often used in the conventional analog controller tuning. When the controlled system has one dominant time constant and other minor time constant, the standard form of the control system transfer function for the modulus optimum is achieved by cancelling the largest time constant, while the closed loop gain should be larger than unity for as high frequencies as possible [19]. This method is widely used because of its simplicity and fast response.

The open loop transfer function of current controller is given as,

$$G_{C,OL}(s) = K_{p,pu}.\left(\frac{1+T_i.s}{T_i.s}\right).\frac{1}{1+T_a.s}.\frac{1}{R_{pu}}.\frac{1}{1+s.\tau_{pu}} \quad (11)$$

The modulus optimum tuning criteria for this system gives the PI controller parameters as,

$$T_i = \tau_{pu} \quad (12)$$

$$K_{p,pu} = \frac{\tau_{pu}.R_{pu}}{2.T_a} \quad (13)$$

This tuning criterion gives the open loop and closed loop transfer functions of the current control loop as follows.

$$G_{C,OL}(s) = \frac{1}{2.T_a}.\frac{1}{s.(1+T_a.s)} \quad (14)$$

$$G_{C,CL}(s) = \frac{1}{2T_a{}^2s^2 + 2T_a.s + 1} \quad (15)$$

The resulting system has a frequency of natural oscillation $\omega_n = 1/T_a\sqrt{2}$ and damping factor $\zeta = 1/\sqrt{2}$. Because this method is based on simplification by pole cancellation, and optimizing the absolute value to 1, the resulting response of the system would always correspond to values of ζ and ω_n as above. The system can however, be tuned for a desired value of crossover frequency by choosing total constant gain term of (11) to be equal to the desired crossover frequency. The crossover frequency of current open loop is chosen one or two order smaller than switching frequency of converter to avoid interference from switching frequency noise.

B. Symmetrical Optimum

When the controlled system has one dominant time constant and other minor time constant, the PI controller can be tuned using the modulus optimum criteria as described in previous section. However, when one of the poles is already near to the origin or at the origin itself, the pole shift does not change the situation significantly. The open loop transfer function of the voltage controller already has two poles at the origin. An alternative criterion to tune the controllers in this condition is given by the symmetrical optimum criteria.

A symmetrical optimum design criterion obtains a controller that forces the frequency response of the system as close as possible to that for low frequencies. The method has the advantage of maximizing the phase margin. As phase margin is maximized for given frequency, the system can tolerate more delays, which is important for systems having delays. This method optimizes the control system behaviour with respect to disturbance input. The method has well established tuning rules and has good disturbance rejection [20]. An extended approach of tuning by symmetric optimum [21] is presented here.

From the system block diagram as developed in Fig. 5, the open loop transfer function of the system without considering the feed-forward and the disturbance input is given by,

$$G_{V,OL}(s) = K_{pv,pu}.\left(\frac{1+T_{iv}.s}{T_{iv}.s}\right).\frac{1}{1+T_{eq}.s}.\left(\frac{V_{dpu}}{V_{dcpu}}.\frac{\omega_b.C_{pu}}{s}\right) \quad (16)$$

For given open loop transfer function of the system, cancellation of pole by setting $T_{iv} = T_{eq}$ is impossible as it leads to two poles at origin and the system becomes unstable. Introducing $K = \frac{V_{dpu}}{V_{dcpu}}$ and $T_c = 1/\omega_b.C_{pu}$, the transfer function can be written as,

$$G_{V,OL}(s) = K_{pv,pu}.\left(\frac{1+T_{iv}.s}{T_{iv}.s}\right).\frac{K}{1+T_{eq}.s}.\left(\frac{1}{s.T_c}\right) \quad (17)$$

The tuning criteria according to symmetrical optimum is obtained using the Nyquist criteria [22] of stability,

$$|G_{V,OL}(j\omega)| = 1 \text{ and } \angle G_{V,OL}(j\omega) = -180^o + \Phi_M \quad (18)$$

where Φ_M is the phase margin. Differentiation of the angle criteria with respect to ω gives the condition for maximum value of phase margin, which is,

$$\omega_d = \frac{1}{\sqrt{T_{iv}.T_{eq}}} \quad (19)$$

This condition gives the tuning criteria for time constant of the controller as,

$$T_{iv} = T_{eq}.\left(\frac{1+\sin\Phi_M}{1-\sin\Phi_M}\right) \quad (21)$$

The resulting open loop frequency characteristic will have a maximum phase Φ_M at the crossover frequency of ω_d, symmetric about 1/ T_i and 1/T_{eq}. Then by symmetric property, we can also write,

$$T_{iv} = a^2.T_{eq} \quad (22)$$

where 'a' is the symmetrical distance between 1/ T_{iv} to ω_d, and 1/ T_{eq} to ω_d. Then from the magnitude condition, the tuning for gain of controller can be found as follows.

$$K_{pv,pu} = \frac{T_c}{K.\sqrt{T_{iv}.T_{eq}}} = \frac{T_c}{a.K.T_{eq}} \quad (23)$$

Now using the PI controller parameters, the open loop transfer function and the closed loop transfer function become,

$$G_{V,OL}(s) = \frac{1}{a^3.T_{eq}{}^2.s^2}.\left(\frac{1+a^2.T_{eq}.s}{1+T_{eq}.s}\right) \quad (24)$$

$$G_{v,CL}(s) = \frac{1+a^2.T_{eq}.s}{1+a^2.T_{eq}.s+a^3.T_{eq}{}^2.s^2+a^3.T_{eq}{}^3.s^3} \quad (25)$$

As it is seen that the denominator of the closed loop transfer function has a pole, $s = -1/a.T_{eq}$. Hence, the system can be simplified as follows.

$$G_{v,CL}(s) = \frac{1+a^2.T_{eq}.s}{(a.T_{eq}.s+1).(a^2.T_{eq}{}^2.s^2+a.(a-1).T_{eq}.s+1)} \quad (26)$$

Most of the literature use $T_{iv} = 4T_{eq}(a=2)$ for the optimization according to conventional symmetrical optimum tuning [21]. The resulting performance gives an overshoot of around 43%, settling time around 16.3 T_{eq} and a phase margin of about 36°. The phase margin value is low and the system has a high overshoot, but still the system response is fast. It is possible to compensate the overshoot and enhance the performance of controller by employing a filter in the reference signal. Another option is to choose a higher value of a, so that the phase margin is increased and the damping is also improved, but then, the system response becomes slower. Hence the choice of the controller parameters from design point of view is a compromise between the performances. The recommended

value of the ratio T_{iv}/T_{eq} is constrained between 4 and 16 in literature [23].

From the denominator of the transfer function (26), the eigenvalues to the characteristic equations are,

$$s_1 = \frac{-1}{a.T_{eq}} \tag{27}$$

$$s_2, s_3 = -\left(\frac{a-1}{2.T_{eq}}\right) \pm \sqrt{\left(\frac{a-1}{2.a.T_{eq}}\right)^2 - \left(\frac{1}{a.T_{eq}}\right)^2} \tag{28}$$

This generalization shows three conditions for roots s_2,s_3:

- a <3, the roots are complex conjugate.
- a =3, roots are real and equal
- a >3, roots are real and distinct.

Thus for a given value of T_{eq}, if 'a' is varied, the roots start from complex conjugate roots on imaginary axis for a=1, and move away from imaginary axis, becoming real and equal at a=3 and if increased further, the roots move along the real axis. The damping factor can be changed by varying 'a'. So the value of 'a' can be chosen for the condition fulfilling desired performance. The specifications could be the cross-over frequency at which the phase margin is maximum, or the value of desired phase margin. However, the specifications should result in the value of 'a' in the acceptable region.

There are no explicit specification of performance indicators like damping factor or settling time, and it is difficult to analytically express these performances in terms of 'a', as the closed loop system is a third order system. However, for closed loop system (26), if the real pole is located very far from the origin, transients corresponding to such remote pole are small, last for short time and can be neglected. The system can then be approximated by a second order system, for an easier estimate of response characteristics. But when specifying 'a', there is no control over relative spacing of the real pole and the complex poles, so such a simplification and degree of freedom can not be achieved.

C. Pole placement interpretation of Symmetric Optimum

Using the symmetric optimum method, controllers can be tuned for variable damping by specifying the value of a, but the range of variation is very small. Lower values of 'a' give a small phase margin and high oscillations, while increasing values of 'a' may lead to better damping but slower response. Symmetrical optimum method can be extended so as to specify damping factor for the system as part of tuning procedure using pole placement [23].

This method considers the special case when a <3, that is the characteristic equation has one real root, p and a pair of complex conjugate root, $\sigma \pm j\omega$. Then it results in a characteristic equation,

$$s^3 + (p+2\sigma).s^2 + (2p\sigma + \sigma^2 + \omega^2).s + p.(\sigma^2 + \omega^2) \tag{29}$$

The real pole placement is defined through a relation,

$p = \alpha.\sigma$ where α >1.

and for the complex roots, the relation between damping factor and the roots is defined as

$$\omega^2 = \frac{1-\zeta^2}{\zeta^2}.\sigma^2 \tag{30}$$

Then, the characteristic equation is,

$$s^3 + (\alpha+2).\sigma.s^2 + \left(2\alpha + 1 + \frac{1-\zeta^2}{\zeta^2}\right).\sigma^2.s + \left(1 + \frac{1-\zeta^2}{\zeta^2}\right).\sigma^3 \tag{31}$$

But the characteristic equation of the system (17) is,

$$s^3 + \frac{1}{T_{eq}}.s^2 + \frac{K_p.K}{T_c.T_{eq}}.s + \frac{K_p.K}{T_i.T_c.T_{eq}} \tag{32}$$

Equating the coefficients of (31) and (32), the controller parameters can be found in terms of α and ζ. And, specifying ζ for calculating controller parameters has more explicit physical meaning than specifying 'a' as in previous case.

V. Application of Tuning Relations

Considering the system given in [7], with system parameters L_{pu} = 0.15, C_{pu}= 0.88, R_{pu} = 0.01 and ω_b = 377, the cases of parameter tuning of the controller are presented using the tuning rules of modulus optimum, symmetric optimum and explicit damping factor specification. The switching frequency of the converter block (f_{switch}) is taken as 10kHz. Average time delay of converter is then

$$T_a = \frac{T_{switch}}{2} = \frac{1}{2.f_{switch}} \tag{33}$$

A. Tuning of current controller using modulus optimum

The current controller was tuned using modulus optimum criteria.

Controller gain, $K_{p,pu}$ = 3.9788

Integral time constant, T_i = 0.039788

The open loop transfer function as shown in Fig. 7 had a phase margin of 65.5° and gain margin infinity showing the closed loop system to be stable.

The time response to step input was studied, which gave the results as in Fig. 8.

Maximum Overshoot, M = 1.042

Time for maximum overshoot, t_m = 0.0003s

Settling time, using 2%criteria, t_s = 0.0004s

The open loop bode plot gives the open loop crossover frequency of 9.1×10^3 rad/s (1.448 kHz), which is about 7 times smaller than the switching frequency of 10 kHz, indicating acceptable ratio [16].

B. Tuning of voltage controller using symmetric optimum

For the steady state operating conditions, $V_{dpu} = V_{dcpu}$ =1pu, and choosing a =3, the controller parameters are tuned according to symmetrical optimum condition.

Controller gain, $K_{pv,\,pu}$ = 10.0474

Integral time constant, T_{iv} = 0.0009

The bode plot of open loop transfer function in Fig.9 shows stable operating limits with a maximum phase margin of 53.1° , occurring at the crossover frequency of 3.33×10^3 rad/s (530.5Hz).

The step response of the system is shown in Fig.10 which has following characteristics:

Maximum Overshoot, M = 1.25

Time for maximum overshoot, t_m = 0.0009s

Settling time, using 2%criteria, t_s = 0.0024s

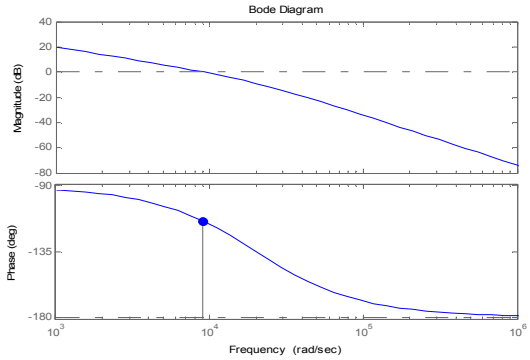

Fig. 7. Open loop Bode plot of current controller transfer function

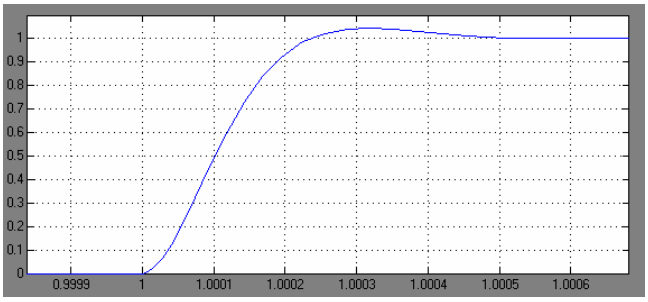

Fig. 8.Step response of Current controller tuned with modulus optimum

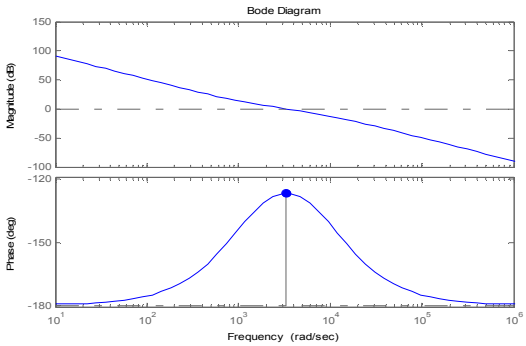

Fig. 9. Open loop Bode plot of voltage controller transfer function tuned with symmetric optimum

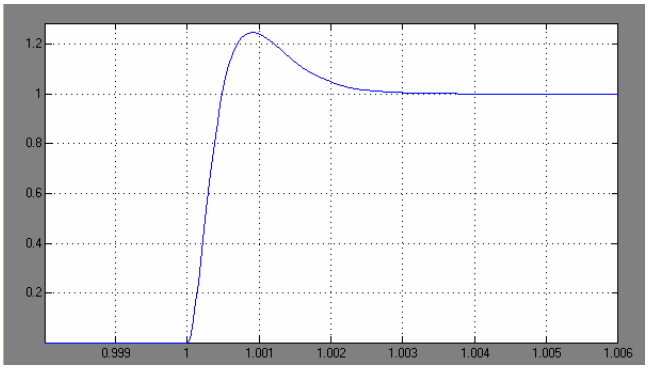

Fig.10. Step response of Voltage controller tuned with symmetric optimum

C. *Tuning of voltage controller using pole placement of symmetric optimum*

Tuning voltage controller using pole placement is just a special case of tuning using symmetric optimum, where the

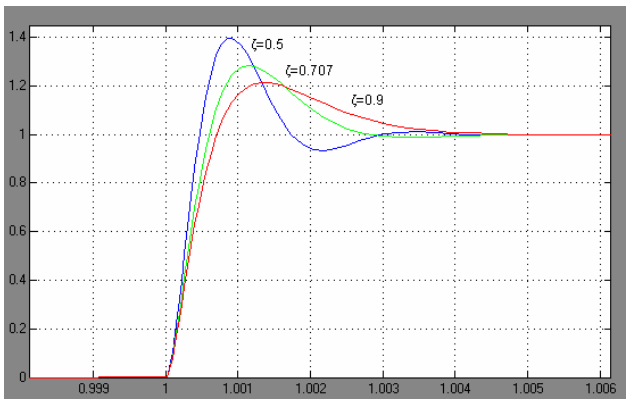

Fig. 11. Step response for fixed value of α=5, and varying ζ = 0.5, 0.707 and 0.9

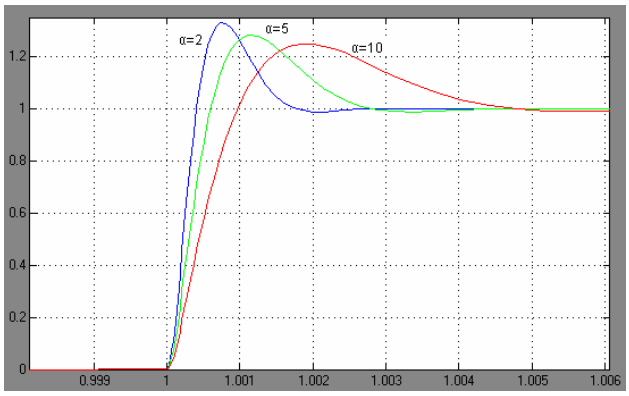

Fig.12. Step response for fixed value of ζ =0.707, and varying α = 2, 5 and 10

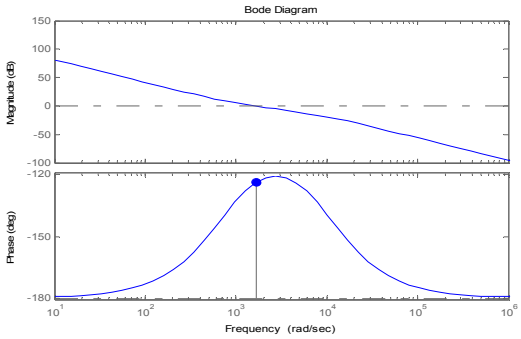

Fig. 13. Open loop Bode plot of voltage controller transfer function when tuned with pole placement

placement of the real pole and the damping of complex pole can be specified. There are two parameters α and ζ that can be specified for a desired performance and the variation of step response with these parameters are shown in Fig. 11 and 12. It is seen that by specifying the damping factor of the complex poles, the overshoot in the step response of third order system can be changed. With increasing ζ, the overshot is decreased and the speed of response is slightly decreased. On the other hand, for a given value of ζ increase in α seems to make the response slow with slight decrease in overshoot.

For a particular case of α=10 and ζ=0.707, the controller parameters were tuned by pole placement resulting in,

Controller gain, $K_{pv,\,pu}$ = 4.6052

Integral time constant, T_{iv} = 0.0013196

The open loop bode plot of the system in Fig.13 shows a stable operation with phase margin 56° at crossover frequency of 1.66×10^3 rad/s (264.19Hz).

The time domain response of the system to step input has the following response:

Maximum Overshoot, M = 1.25

Time for maximum overshoot, t_m = 0.0019s

Settling time, using 2%criteria, t_s = 0.0043s

As compared to symmetric optimum, the tuning of controllers using pole placement method results in a slower response. But still the speed of response is acceptable. In this method by specifying α and ζ the closed loop poles of the system are configured. However, as it is a special case when the closed loop system has a pair of complex poles, there is not much freedom in choosing the pole-zero configurations. The advantage of this method might be stated as the explicit specification of damping ratio and pole-zero configurations, that has better implications than specification of parameter '*a*' in normal case.

VI. Discussion of Tuning Criteria

Adjustment of current controller according to modulus optimum provides good response with small overshoot to a step change of reference. Because of the cancellation of slow process pole by the controller zero, the response is considerably improved. If set point responses are predominant factor of concern, pole-zero cancellation might be right, but if load responses or disturbance rejection are also important, this method may not be sufficient [24]. The cancellation controller has good set point response but leads to a very slow disturbance response, because system poles are not altered in the disturbance transfer function, resulting controller zero to become poles in disturbance transfer function [25]. In addition to that, an inexact cancellation also results in sluggish response and poor robustness. Moreover, if the time constant of the input system (τ) is large, the integral time constant of the controller will increase. This will also cause the capability of controller for disturbance rejection to become poor. These factors need to be considered in further applications.

Adjustment of voltage controller according to symmetric optimum provides high proportional gain and low integral time constant, which results in fast response as well as strong rejection of disturbance. With this method of tuning, substantial overshoot can be seen in the step response, which might require limiting of rate of change of voltage reference. Moreover, additional filtering might also be required for ripple in dc bus voltage. But again, the additional filtering will decrease the controller gain and the bandwidth. Modification of symmetric optimum using pole placement is possible for the special case where the closed loop system has complex poles. Explicit specification of damping factor for complex poles can be used to specify the closed loop pole-zero configuration and set the response of the system. But as seen from Fig. 13, the resulting system is not the optimum one from the phase margin point of view.

Both of the tuning criteria, modulus optimum and symmetric optimum are based on optimisation of dynamic performance of the controlled system. However, in tuning of PI controllers for HVDC, only considering the dynamic performance is not sufficient.

The control design is based on the assumption that the inner and outer loops are decoupled and hence, can be linearized. Non ideal operating condition leads to generation of harmonics, influencing both ac and dc control. When low order harmonics are present in the system, the two control loops cannot be considered decoupled. The current loop is designed considering constant dc bus voltage because the voltage control loop is much slower than the inner current control loop. If dc voltage has low frequency ripple, it cannot be considered constant for current loop design.

In order to investigate the possible problems to be encountered in VSC-HVDC installation, detailed analysis of dynamic behaviour of the system and development of suitable controllers to overcome the problems are needed. The tuning rules of the controllers should be devised to reduce negative influence on system performance due to non-ideal operating conditions, system non-linearities etc.

VII. Conclusions

A mathematical model of a three phase VSC in synchronous reference frame was presented, and based on the model, current and voltage control of VSC was studied. The tuning methods were investigated for PI controller parameter setting. Method of modulus optimum was used to derive parameters of current regulators, and symmetrical optimum to derive parameters of voltage controller. Some possible problems in tuning were presented and discussed, which will be studied further through simulation to derive general guidelines for tuning controllers for improved performances.

VIII. Further Work

A good understanding of control strategies, and control system, their drawbacks and advantages in most general operating conditions, is necessary to derive the most relevant option for control. In further work, analysis of control system and controller tuning will be continued. With the development of the control platform, the controllers will be tested under several circuit conditions, to test the capability and robustness of the controller to handle the adverse situations. The simulation platform will be built in PSCAD to study the control system under different conditions of load disturbances, unbalance conditions etc. with different tuning rules. The simulation results would be studied for verification of operating range, and for severe disturbances to test control robustness. Effect of nonlinearities and unbalanced voltage conditions will also be studied through simulations. This work will be directed to the establishment of general guidelines for tuning the controllers and suggestions for improving the controller performances.

APPENDIX

A. *Park and Clark transformation system*

Transformation	Transforms	Matrix for transformation
Clark transformation	from *abc* to *αβ*	$\frac{2}{3}\cdot\begin{pmatrix} 1 & -1/2 & -1/2 \\ 0 & \sqrt{3}/2 & -\sqrt{3}/2 \end{pmatrix}$
Inverse Clark transformation	from αβ to *abc*	$\begin{pmatrix} 1 & 0 \\ -1/2 & \sqrt{3}/2 \\ -1/2 & -\sqrt{3}/2 \end{pmatrix}$
Park transformation	from *αβ* to *dq*	$\begin{pmatrix} \cos\theta & \sin\theta \\ -\sin\theta & \cos\theta \end{pmatrix}$
Inverse Park transformation	from *dq* to *αβ*	$\begin{pmatrix} \cos\theta & -\sin\theta \\ \sin\theta & \cos\theta \end{pmatrix}$

B. *Base values for Per Unit System*

The following base system is chosen for conversion of the system into Per Unit (p.u.) representation.

S_b = Nominal three-phase power of the ac-grid

V_b = Nominal peak phase voltage at the ac side [$V_{peak.ph}$]

$= \sqrt{\frac{2}{3}}.V_{LL,rms}$ where $V_{LL,rms}$ =Line-Line RMS Voltage

I_b = Nominal peak phase current $= \frac{2}{3}.\frac{S_b}{V_b}$

Z_b = Base ac impedance= $\frac{V_b}{I_b}$

ω_b = Base frequency

The base for per unit transformation is chosen as to achieve a power invariant transformation, so that the ac and dc side power is the same.

As, $S_{3phase} = 3.V_{phase}.I_{phase}$ and then the power balance gives,

$$S_b = \frac{3}{2}.V_b.I_b = V_{dcbase}.I_{dcbase}$$

The base value for dc voltage is chosen as,

$$V_{dcbase} = 2.V_{peak,ph} = 2.V_b ,$$

Then by the power balance equation as above,

$$I_{dcbase} = 3/4 .I_b$$

And, Z_{dcbase} = Base dc impedance= $\frac{V_{dcbase}}{I_{dcbase}} = \frac{8}{3}.Z_b$

REFERENCES

[1] ABB publication, "Its Time to Connect", http://www.abb.com/cawp/gad02181/c1256d71001e0037c1256893005121c7.aspx

[2] Costa Papadopoulas et al, "Interconnection of Greek islands with dispersed generation via HVDC Light technology", ABB

[3] http://www.siemens.com/page/1,3771,1007570-1-12_0_0-0,00.html

[4] F.Schettler, H.Huang and N.Christl, "HVDC transmission systems using voltage sourced converters - design and applications", *IEEE Summer Power Meeting*, July 2000, Vol.2, pp 715-720.

[5] De Donker, R. W. and Novotny, D. W., "Universal Field Oriented Controller", *IEEEYIAS Annual Conference Record*, Pittsburgh, 1988, pp. 450-456.

[6] Kohachiro Nishi, Tatsuhito Nakajima and Akihiko Yokoyama, "Steady–state stability of shaft torsional oscillation in ac-dc interconnected system with self-commutated converters", Scripta Technica, Electr Eng Jpn, 128(4), 25-37, 1999.

[7] C.Schauder, H. Mehta, "Vector Analysis and Control of Advanced Static Var Compensators", IEE Proceedings-C, Vol.140, No.4, July 1993.

[8] Marta Molinas, Bjarne Naess, William Gullvik, Tore Undeland, "Robust Wind Turbine system against Voltage sag with induction generators interfaced to the grid by power electronic converters", IEEJ Trans. IA, Vol 126, No 7, 2006.

[9] R Pena, J C Clare, G M Asher, "Doubly fed induction generator using back to back PWM converters and its application to variable speed wind energy generation", IEE Proc.-ElectrPower Appl., Vol 143, No 3, May 1996.

[10] Ruihua Song et al, "VSC based HVDC and its control strategy", IEEE/PES Trans. and Distrb. Conference and Exhibition, 2005.

[11] J. Svensson, "Synchronisation methods for grid-connected voltage source converters," Proc. Inst. Electr. Eng.-Gener. Transm. Distrib., vol. 148, no. 3, pp. 229–235, May 2001.

[12] S.-K. Chung, "Phase-locked loop for grid-connected three-phase power conversion systems," Proc. Inst. Electr. Eng-Electron. Power Appl.,vol.147, no. 3, pp. 213–219, May 2000.

[13] F. N. Gakis, S. A. Papathanassiou, "Simple control schemes for grid-connected three-phase voltage-source inverters of DG units", Proc.XVII International Conference on Electrical Machines, ICEM'2006, 2-5Sept.2006 Chania, Greece.

[14] Chandra Bajracharya, "Control of VSC-HVDC for wind power", Specialization project, NTNU, Jan. 2008.

[15] Ned Mohan, Tore M. Undeland and W. P. Robbins, Power Electronics: Converters, Applications and Design, John Wiley and Sons Inc.

[16] Ned Mohan, Electric Drives: An Integrative Approach, MNPERE, 2003, pp8-18.

[17] M. Liserre, "Innovative control techniques of power converters for industrial automation", PhD Thesis, Politecnico di Bari, Italy, Dec. 2001.

[18] W. Leonhard, Introduction to Control Engineering and Linear control Systems, New Delhi, 1976.

[19] Â. J. J. Rezek, C. A. D. Coelho, J. M. E. Vicente, J. A. Cortez, P. R. Laurentino, "The Modulus Optimum (MO) Method Applied to Voltage Regulation Systems: Modeling, Tuning and Implementation", Proc. International Conference on Power System Transients, IPST'01, 24-28 June 2001, Rio de Janeiro, Brazil.

[20] O. Aydin, A. Akdag, P. Stefanutti, N. Hugo, "Optimum Controller Design for a Multilevel AC-DC Converter System", Proc. Of Twentieth Annual IEEE Applied Power Electronics Conference and Exposition, APEC 2005, 6-10 March 2005, Vol. 3, pp. 1660-1666

[21] S. Preitl, R.-E. Precup, "An Extension of Tuning Relations after symmetrical Optimum Method for PI and PID Controllers", Automatica, Vol. 35, 1999, pp 1731-1736.

[22] K. Ogata, Modern Control Engineering, Prentice Hall International.

[23] M. Machaba, M. Braae, "Explicit Damping Factor Specification in Symmetrical Optimum Tuning of PI Controllers", Proc. of First African Control Conference, 3-5 Des. Cape Town, South Africa, pp. 399-404.

[24] C. C. Hang, "The Choice of Controller Zeros," IEEE Control Systems Magazine, Vol. 9, No. 1, Jan. 1989, pp.72-75

[25] R. N. Clark, "Another Reason to Eschew Pole-Zero Cancellation," IEEE Control Systems Magazine, Vol.8, No. 2, April 1988, pp. 87-88.